communications biology

A Nature Portfolio journal

Article

https://doi.org/10.1038/s42003-025-09217-y

Synergistic mechanisms of medullary cholinergic-serotonergic pathway interactions in regulating neuronal excitability and locomotor activities

Yi Cheng [1,2], Yue Dai [1,3] ✉, Renkai Ge[4] & Qiang Zhang[5]

Medullary serotonergic (5-HT) neurons play a pivotal role in locomotor initiation. While these neurons receive cholinergic innervation, the functional consequences and underlying mechanisms remain poorly understood. Using *ePet-EYFP* transgenic mice (P3–P6) and multidisciplinary approaches, we elucidated the mechanisms by which cholinergic signaling regulated medullary 5-HT neuronal activity and locomotor output. Key findings included: (1) acetylcholine (ACh) elicited location-dependent excitatory, inhibitory, or neutral responses in 5-HT neurons, recapitulated by muscarine and abolished by atropine, indicating muscarinic receptor (mAChR)-mediated regulation. (2) 5-HT neurons in parapyramidal region exhibited ACh-induced excitation, whereas those in midline raphe nuclei displayed inhibition. (3) ACh-enhanced excitability was mediated via M3 receptors, whereas ACh-induced suppression depended on M2/M4 receptor activation. (4) In vitro bath application of muscarine to medullary region induced triphasic modulation of fictive locomotion. Blockade of M1/M5 receptors did not affect locomotion, whereas M3 receptor antagonism reduced gait velocity and perturbated locomotor rhythm. Conversely, M2/M4 receptor antagonism increased stepping frequency without altering locomotor pattern. This study provided the first mechanistic dissection of how medullary cholinergic-serotonergic interactions regulated neuronal excitability and locomotion, uncovering distinct mAChR subtype contributions to motor control.

Locomotor activity is a complex process requiring neural circuits in brainstem and spinal cord that endogenously generate periodic motor commands for movement[1–3]. Mesencephalic locomotor region (MLR) initiates, maintains, and stops locomotion as well as controls locomotor speed and direction[2,4–7]. Central pattern generator (CPG) in the spinal cord performs and operates locomotion[8–10]. The MLR initiates locomotion through descending pathway to reticulospinal neurons (RSNs) in the pons and medulla, which project to the spinal cord[11–13]. Several studies have reported that serotonergic (5-HT) neurons in medulla are activated by synaptic inputs from the MLR and then release 5-HT in the spinal cord to facilitate generation of locomotion. This MLR-evoked locomotion can be blocked by a 5-HT_7 receptor antagonist (SB 269970)[7,14]. The role of 5-HT in generating locomotion in the spinal cord has been studied extensively by using isolated preparations of neonatal rodents[15,16]. These studies have reported that medullar 5-HT neurons, which act as the interface between MLR and CPG, play a crucial role in signal transmission from the MLR to spinal cord to release 5-HT for locomotion[17,18]. Medullar 5-HT neurons can be classified into two clusters, the parapyramidal region (PPR) and the midline raphe nuclei (MRN). In previous study we systematically studied the persistent inward currents (PICs) in 5-HT neurons of medulla in ePet-EYFP mice and characterized PICs on the basis of their electrophysiological and ionic properties[19–22]. However, the intrinsic membrane properties and morphological characteristics of 5-HT neurons in the medulla and their role in regulating locomotion are not clear yet.

[1]Key Lab of Adolescent Health Assessment and Exercise Intervention of Ministry of Education, College of Physical Education and Health Care, East China Normal University, Shanghai, China. [2]Department of Physical Education, Kunming Medical University, Kunming, China. [3]Shanghai Key Laboratory of Multidimensional Information Processing, School of Communication and Electronic Engineering, East China Normal University, Shanghai, China. [4]School of Physical Education and Health Care, East China Jiaotong University, Nanchang, China. [5]School of Electrical and Information Engineering, Jiangsu University of Science and Technology (Zhangjiagang Campus), Zhangjiagang, China. ✉e-mail: ydai@tyxx.ecnu.edu.cn

Several neurotransmitter systems play an essential role in modulating the neural activity during locomotion[16,23–26]. Cholinergic system is one of them which acts at both the brainstem and spinal cord[24,27,28]. In vertebrate spinal cord, exogenously applied acetylcholine (ACh) induces fictive locomotion in the isolated spinal cord[29], while the inherent cholinergic inputs strongly modulate the activity of interneurons and motoneurons to control the locomotor output[30–33] via activating M2 and M3 muscarinic receptors (mAChRs)[34,35]. In the vertebrate midbrain, cholinergic neurons in the MLR are shown to be indispensable for limb movement[5,36]. Bath application of ACh or mAChRs agonists, pilocarpine, to the brainstem evokes locomotion, which can be blocked by atropine[37]. Recent studies show ACh regulates medullary 5-HT neuron PICs via mAChRs, with M3 receptor activation enhancing them[20]. The above studies suggest that mAChRs expressed in both the spinal cord[38,39] and brainstem[40] are essentially involved in regulation of motor output and locomotion in vertebrates. However, little is known about the mechanism by which the mAChRs in the brainstem regulates the motor activities. The purpose of this study is to investigate the synergistic interactions between cholinergic and serotonergic pathways in the brainstem and their mechanistic roles in regulating neuronal excitability and locomotor activities in mice.

Using multiple approaches, we characterized the medullar 5-HT neurons in the mice and discovered that ACh induced varying effects on the 5-HT neurons. The ACh-increased excitability of 5-HT neurons was mediated by activation of M3 receptors while the ACh-reduced excitability was produced by activation of M2 and M4 receptors. We further revealed that the mAChRs of medullary 5-HT neurons play a crucial role in rhythmic generation during fictive locomotion.

Results

Characterization of the serotonergic neurons in the medulla of *ePet-EYFP* mice

In the present study, we characterized 5-HT neurons in the entire brainstem. The distribution of 5-HT neurons from ventral and midsagittal slices of the brainstem were shown in the transverse medullar slices in Fig. 1A1 (please also see Supplementary Fig. 1A1–A4) and sagittal brainstem slices in Fig. 1A2 (also see Supplementary Fig. 1B1-B4). 5-HT neurons were mainly distributed in three regions of brainstem: the midbrain, pons, and medulla in Fig. 1A2 (also see Supplementary Fig. 1B).

Transverse slices were used to study the intrinsic membrane properties and morphology of 5-HT neurons in medulla (Fig. 1A1). The electrophysiological data were collected from 146 5-HT neurons of P3-P6 *ePet-EYFP* mice in the present study. Significant differences were found in both the resting membrane potential (RMP) and input resistance (Rin) of 5-HT neurons between the parapyramidal region (PPR) and midline raphe nuclei (MRN). The RMP was more depolarized in PPR neurons (PPR: −63.4 ± 6 mV vs MRN: −65.5 ± 5 mV; $p = 0.03$), and Rin was significantly lower in PPR neurons (PPR: 1069.5 ± 506 MΩ vs MRN: 1294.9 ± 677 MΩ; $p = 0.04$). All other measured active and passive properties showed no significant regional differences (PPR, $n = 99$; MRN, $n = 47$; Supplementary Table 1). We also studied morphology of 5-HT neurons labeled by intracellular fluorescent dye of 3% tetramethylrhodamine. The fluorescent images were analyzed by Sholl analysis technology (Supplementary Fig. 2A and B).

Compared to MRN 5-HT neurons ($n = 14$), 5-HT neurons in the PPR ($n = 17$) (Fig.1 B–D) exhibited a bigger diameter ($P < 0.05$), soma area ($P < 0.05$), soma volume ($P < 0.05$), and total branch length ($P < 0.01$, Fig.1D1–D4). Statistical results also showed that the PPR 5-HT neurons had a bigger number of primary segments, branch points, and branches than MRN 5-HT neurons ($P < 0.01$, Fig. 1D5). Typically, the PPR 5-HT neurons had a bigger number of intersections than the MRN 5-TH neurons within the range of 50 μm apart from soma ($P < 0.05$, Fig. 1D6). Detailed data were presented in Supplementary Table 2. These data indicated that neurons in the PPR region had more abundant dendrites than MRN region.

The morphology of medullary 5-HT neurons can also be divided into bipolar and multipolar neurons. Results showed that 74.2% 5-HT neurons (23/31) were multipolar neurons (Fig. 2A cell1 to cell4) and 25.8% neurons (8/31) bipolar neurons (Fig. 2A cell5 and cell6). Multipolar neurons could be further divided into two types, pyramidal neurons with conic shaped soma and large apical dendrite (Fig. 2A cell1 and cell2), and stellate neurons with radial dendrites (Fig. 2A cell3 and cell4). Statistical results indicated that number of intersections of stellate neurons were more than that of pyramidal and bipolar neurons, especially in the range of 50 μm apart from soma (Fig. 2B1, $p < 0.05$). The three types of neurons also exhibited significant differences in primary segments, branch points, number of branches, and diameters (Fig. 2B2 and B3). No significant difference was found in soma area (Fig. 2B4), soma volume (Fig. 2B5), and total branches length (Fig. 2B6) of three types of 5-HT neurons (See Supplementary Table 3 for details). We further classified the regional distribution of the three morphological subtypes. The results demonstrated that stellate neurons were predominantly located in the PPR (11/16, 68.8% of all stellate neurons), whereas bipolar neurons were enriched in the MRN (6/8, 75.0% of all bipolar neurons). Pyramidal neurons, however, showed no strong regional bias (PPR: 4/7 vs. MRN: 3/7) (Fig. 2B7).

We further compared the membrane properties of three types of 5-HT neurons (Fig. 2C). The results showed that the Rin of bipolar neurons was significantly greater than that of pyramidal cells and stellate cells (Fig. 2C5). Furthermore, no significant differences were observed among the three types of neurons in RMP (Fig. 2C1), rheobase (Fig. 2C2), action potential (AP) height (Fig. 2C3), or afterhyperpolarization (AHP) depth (Fig. 2C4). In summary, these data indicated that medullary 5-HT neurons were heterogeneous population of neurons. However, the difference in morphology of these neurons did not produce a significant difference in their active membrane properties.

Varying effects of acetylcholine on 5-HT neurons

To determine the regulatory effect of ACh on 5-HT neurons in medulla, we investigated the cellular mechanisms with whole-cell patch-clamp recordings performed in 5-HT neurons of medullar transverse slices. Our data showed that ACh induced three different effects on 5-HT neurons which could be characterized as an increased excitability (Fig. 3A), a decreased excitability (Fig. 3B), and an unchanged excitability of the neurons (Fig. 3C). Bath application of ACh (15 μM) depolarized the RMP and increased neuronal excitability in 55.9% of the 5-HT neurons (38/68). A typical example was given in Fig. 3A1, where the membrane potential of the 5-HT neuron was depolarized by about 15 mV after bath application of 15 μM ACh. ACh also indued a reduction of AP height, AHP depth and Rin (Fig. 3A2 and A3). Analysis of 38 neurons showed that ACh significantly depolarized the RMP and reduced the rheobase, AP height, AHP depth and Rin (Fig. 3A4–A8). On contrary, however, ACh also hyperpolarized the RMP and decreased the neuronal excitability in 11.8% of the 5-HT neurons (8/68). A typical example was shown in Fig. 3B1, where bath administration of 15 μM ACh hyperpolarized the RMP and decreased the AP height and Rin (Fig. 3B2 and B3). Statistical results from 8 neurons showed that ACh significantly hyperpolarized the RMP, increased the rheobase, and decreased the AP height, AHP amplitude and Rin (Fig. 3B4–B8). Finally, experimental results showed that a 32.3% of the 5-HT neurons (22/68) did not respond to ACh significantly. An example was shown in Fig. 3C1–C3, and statistical analysis from 22 neurons indicated that there was no significant difference in RMP, rheobase, AP height, amplitude of AHP and Rin between the control and ACh groups (Fig. 3C4–C8). Detailed data were presented in Supplementary Table 4.

Substantially empirical evidence from previous investigations has revealed that muscarinic acetylcholine receptors (mAChRs) exhibit widespread distribution within the brainstem circuitry and functionally engage in the regulation of neuronal excitability[41,42]. Our previous study indicated that cholinergic modulation of 5-HT neurons in the brainstem was primarily mediated by mAChRs activation[20,43]. In the present study, we further explored the involvement of mAChRs in regulation of 5-HT neurons' excitability with bath application of the non-selective mAChR antagonist atropine (3 μM) in presence of ACh (15 μM) in recording

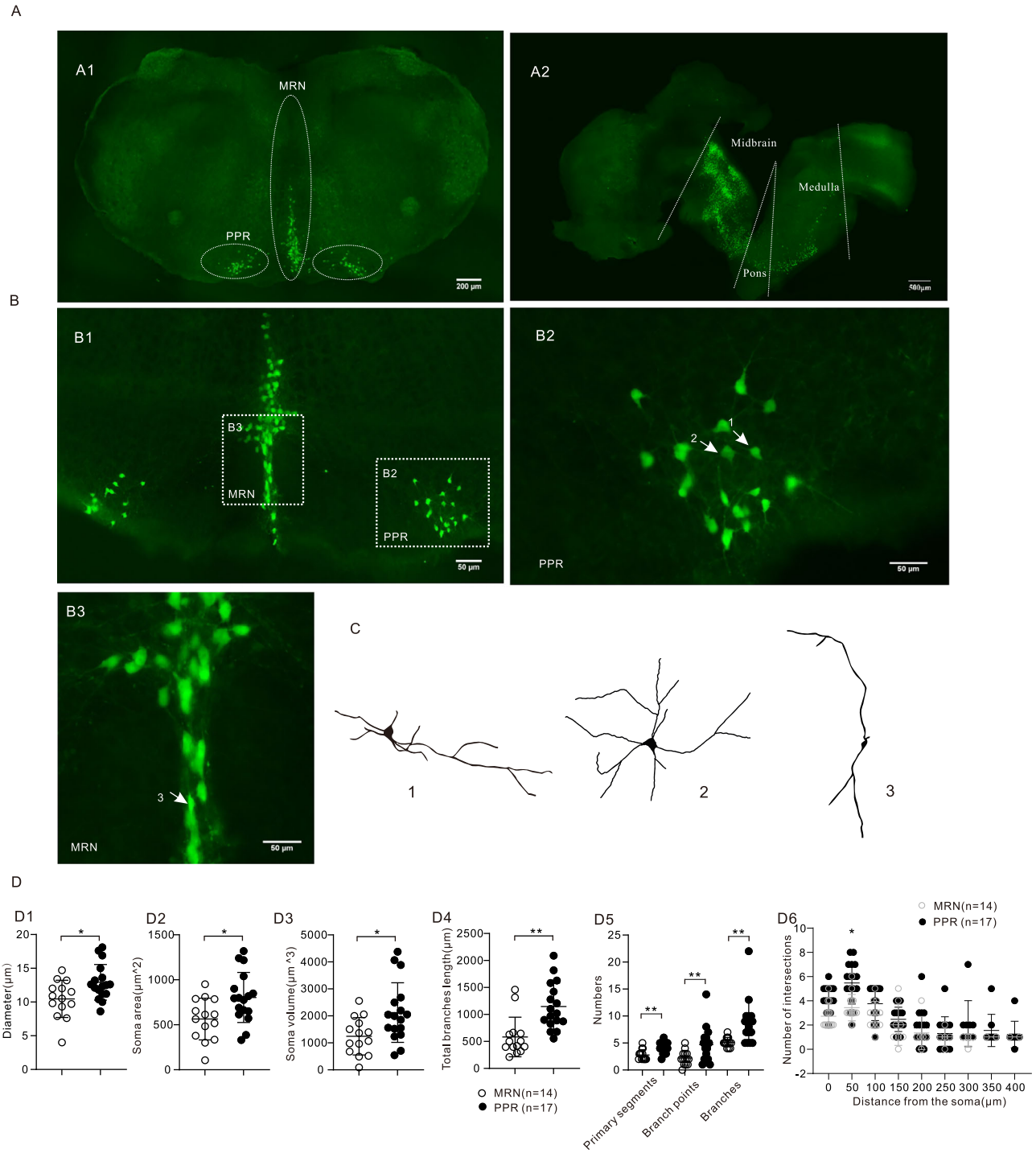

Fig. 1 | Characterization of 5-HT Neurons. A Distribution of serotonergic neurons. A1 Distribution of 5-HT neurons in a transverse slice of the medulla. The dotted circles represent the parapyramidal region (PPR) and midline raphe nuclei (MRN). A2 Distribution of 5-HT neurons in a sagittal slice of the brainstem. The dashed line divides the brainstem into the midbrain, pons, and medulla. **B** Localization of recorded 5-HT neurons **B1** Distribution of 5-HT neurons in transverse section of the medulla. Dashed outlines indicate the boxed regions of PPR expanded in B2 and MRN expanded in B3. **B2** Higher-magnification view of PPR region (boxed in B1) with recorded neurons: Cell 1 and Cell 2. **B3** Higher-magnification view of MRN region (boxed in B1) with recorded neuron Cell 3. **C** Morphology of three cells marked with arrows in B2 and B3, respectively. **D** Summary diagrams showing the diameter (**D1**), soma area (**D2**), soma volume (**D3**), total branch length (**D4**), and the number of primary segments, branch points, and branches (**D5**) of 5-HT neurons from the MRN ($n = 14$) and PPR ($n = 17$). Statistical analysis for D1–D5 was performed using a two-sample heteroscedastic t-test. **D6** Statistical results show significant differences in intersections between PPR and MRN 5-HT neurons, especially in the range of 50–100 μm ($P < 0.05$), analyzed by one-way ANOVA. Error bars represented SD; *: $P < 0.05$, **: $P < 0.01$.

solution (Fig. 3D1 and D3). Our data showed that atropine completely blocked the ACh-induced increased excitability (Fig. 3D1) as well as decreased excitability of 5-HT neurons (Fig. 3D3). Statistical analyses revealed that 3 μM atropine completely suppressed all ACh-induced electrophysiological changes in both neuronal subtypes. In depolarizing neurons ($n = 8$; Fig. 3D2), atropine reversed the ACh-mediated depolarization of the RMP, reduction in rheobase, and decreases in AP amplitude, AHP amplitude, and Rin. Conversely, in hyperpolarizing

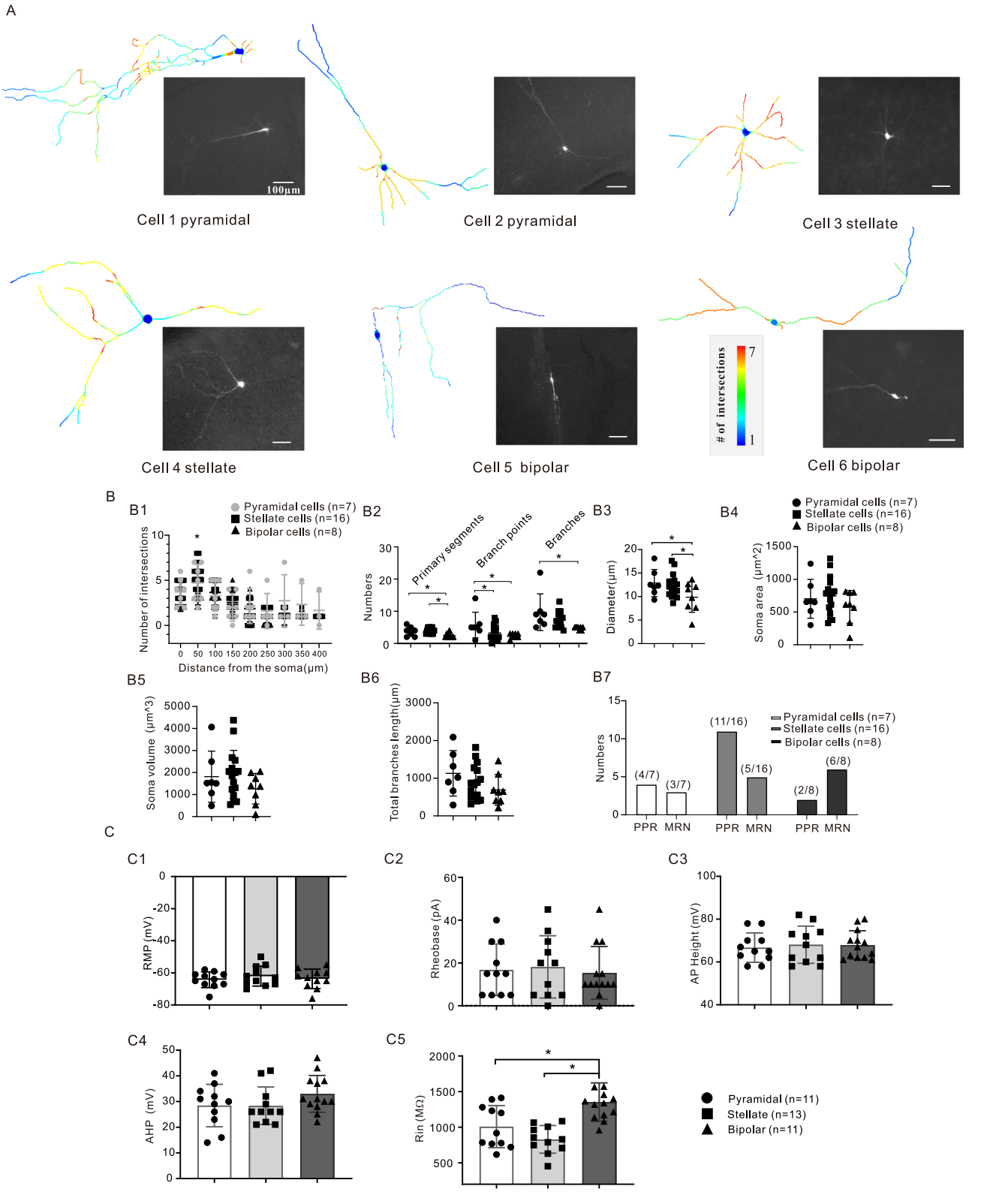

Fig. 2 | Morphology and membrane properties of three types of 5-HT neurons. **A** Based on morphological characteristics, 5-HT neurons were divided into pyramidal neuron (cell 1 and cell 2), stellate neuron (cell 3 and cell 4) and bipolar neuron (cell 5 and cell 6). **B** Morphological differences among three types of 5-HT neurons. B1. Statistical results showed that intersections were obviously different in pyramidal, stellate and bipolar 5-HT neurons, especially in the range of 50–100 μm ($p < 0.05$). **B2** Graphs show the numbers of primary segments, branch points and branches of pyramidal, stellate and bipolar neuron. **B3**–**B6** Summary diagrams show the diameter length (**B3**), soma area (**B4**), soma volume (**B5**), total branches length (**B6**) of pyramidal ($n = 7$), stellate ($n = 16$) and bipolar ($n = 8$) 5-HT neuron. **B7** Summary diagram shows the regional distribution of the three morphological subtypes, indicating that stellate neurons were predominantly located in the PPR (11/16, 68.8%), while bipolar neurons were mainly distributed in the MRN (6/8, 75.0%). Pyramidal neurons showed no significant regional preference (PPR: 4/7 vs. MRN: 3/7). **C** Summary diagrams show the resting membrane potential (RMP, **C1**), rheobase (**C2**), action potential (AP) height (**C3**), afterhyperpolarization (AHP) depth (**C4**), and input resistance (Rin, **C5**) of pyramidal ($n = 11$), stellate ($n = 13$) and bipolar ($n = 11$) 5-HT neuron. Analyzed by one-way ANOVA, error bars represented SD; ∗: $P < 0.05$.

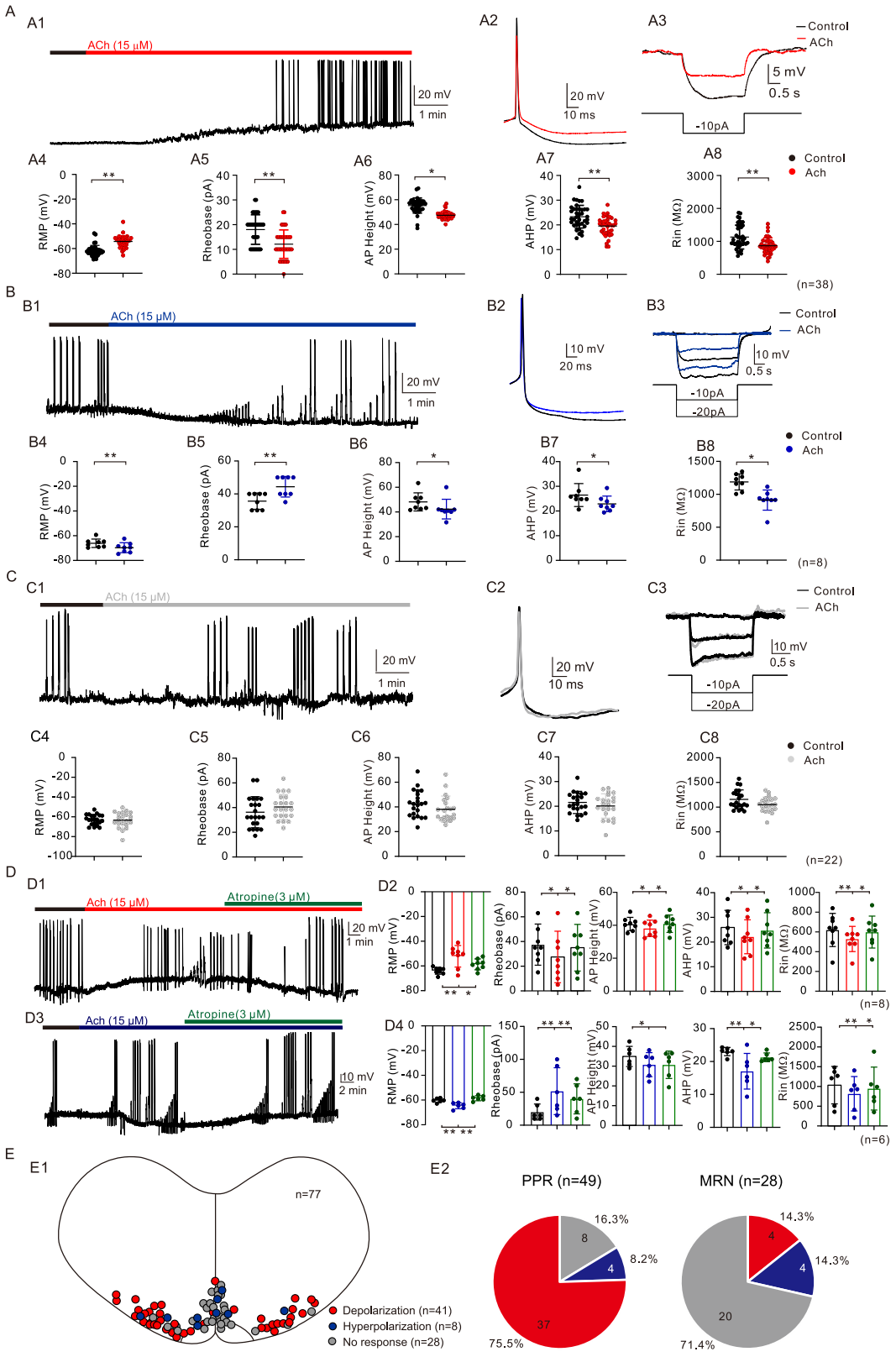

neurons ($n = 6$; Fig. 3D4), atropine prevented ACh-induced hyperpolarization of the RMP, increase in rheobase, and reductions in AP amplitude, AHP amplitude, and Rin. The above results suggested that ACh modulation of 5-HT neurons was involved in a complex cellular mechanism, where the mAChRs played a dominate role. See Supplementary Table 5 for detailed data.

We systematically described the distribution of medullar 5-HT neurons based on their different responses to ACh in terms of increased excitability (RMP depolarization), decreased excitability (RMP hyperpolarization) and unchanged excitability (RMP unchanged) of the neurons (Fig. 3E1). Statistical results indicated that ACh induced RMP depolarization (ΔEm>0), RMP hyperpolarization (ΔEm<0) and unchanged RMP

Fig. 3 | The modulation of acetylcholine (ACh) on 5-HT neuron excitability. **A** ACh increased the excitability of 5-HT neurons. **A1** ACh induced membrane potential depolarization. **A2** ACh decreased AP height and amplitude of AHP. **A3**. ACh decreased Rin. **A4–A8** Summary diagrams showed ACh-induced significant changes in the membrane properties including RMP, rheobase, AP height, AHP depth and Rin recorded in control (black) and presence of 15 μM ACh (red) ($n = 38$). **B** ACh decreased the excitability of 5-HT neurons. **B1** ACh induced membrane potential hyperpolarization. **B2**. ACh decreased AP height and amplitude of AHP. **B3** ACh decreased Rin. **B4–B8** Summary diagrams showed ACh -induced significant changes in the membrane properties including RMP, rheobase, AP height, AHP depth and Rin recorded in control (black) and presence of 15 μM ACh (blue) ($n = 8$). **C** ACh did not substantially changed the excitability of 5-HT neurons. ACh did not induced significant change in membrane potential (**C1**), AP height and amplitude of AHP (**C2**) and Rin (**C3**). **C4–C8** Summary diagrams showed ACh did not induce substantial change in the membrane properties of RMP, rheobase, AP height, AHP depth and Rin which were recorded in control (black) and presence of 15 μM ACh (grey) ($n = 22$). Statistical analysis for panels A-C was performed using paired-sample t-tests. **D** Muscarinic receptor was involved the modulation of ACh on 5-HT neurons. **D1** ACh-mediated RMP depolarization were blocked by atropine. **D2**. Statistical results listed for the RMP, Rheobase, AP height AHP depth and Rin of 5-HT neurons in control (black), 15 μM ACh (red) and 3μM atropine (green), respectively. **D3**. ACh-mediated RMP hyperpolarization were blocked by atropine. **D4** Statistical results summarized for the RMP, Rheobase, AP height AHP depth and Rin of 5-HT neurons recorded in control (black), 15 μM ACh (blue) and 3 μM atropine (green). Statistical analysis for panel D was performed using one-way ANOVA. **E** ACh effects on 5-HT neuron RMP in the medulla. **E1** Three type effects induced by ACh on the RMP of 5-HT neurons and their medullary distribution. **E2** Proportions of three type effects by ACh on the RMP in PPR and MRN, respectively. Error bars represented SD; ∗: $P < 0.05$, ∗∗: $P < 0.01$.

(ΔE = 0) in 75.5%, 8.2%, 16.3% of 5-HT neurons ($n = 49$), respectively, in the PPR, while the ACh-produced depolarization, hyperpolarization and unchanged RMP were 14.3%, 14.3% and 71.4% of 5-HT neurons ($n = 28$), respectively, in the MRN (Fig. 3E2). These results demonstrated that ACh-increased excitability of 5-HT neurons were mainly observed in PPR whereas the unchanged excitability was primarily expressed in MRN, suggesting that the effects of ACh on medullar 5-HT neurons were location-dependent. This organization could allow the 5-HT neurons in the PPR and MRN to play different functional roles in generating locomotion with ACh modulation.

Muscarine mimics the regulatory effects of ACh on 5-HT neurons

Based on the above experiment results, we further examined the effects of muscarine on 5-HT neurons of medulla. Following a bath application of muscarine (20 μM), the 5-HT neurons displayed three different changes in membrane potentials including 54.4% depolarized (99/182 cells, Fig. 4A1), 14.3% hyperpolarized (26/182, Fig. 4B1), and 31.3% unchanged RMP (57/182, Fig. 4C1), respectively, in the neurons of PPR and MRN regions.

An example was given in Fig. 4 A1, where 20 μM muscarine evoked repetitive firing (Fig. 4A2) and depolarized the membrane potential with a reduction of Rin (Fig. 4A3) and AHP depth (Fig. 4A4) in a 5-HT neuron. The muscarine-induced depolarization was observed in 54.4% of 5-HT neurons (99/182) (Fig. 4A5), accompanied with a decrease in rheobase (Fig. 4A6), AP height (Fig. 4A7), AHP depth (Fig. 4A8) and Rin (Fig. 4A9). On the other hand, however, the muscarine-induced hyperpolarization of membrane potentials also observed in the medullar 5-HT neurons (Fig. 4B1). As shown in Fig. 4B, 20 μM muscarine hyperpolarized membrane potential (Fig. 4B1), increased rheobase (Fig. 4B2) and reduced Rin (Fig. 4B3) and AHP depth (Fig. 4B4). Statistical results from 26 neurons indicated that muscarine significantly hyperpolarized the RMP (Fig. 4B5) with an increase in rheobase (Fig. 4B6) and a decrease in AP height (Fig. 4B7), AHP depth (Fig. 4B8) and Rin (Fig. 4B9). Similar to the results with ACh, there was a small portion of 5-HT neurons which did not substantially respond to muscarine (Fig. 4C). A typical example was shown in Fig. 4 C1, where 20 μM muscarine did not substantially affect the RMP (Fig. 4C1), rheobase (Fig. 4C2), Rin (Fig. 4C3) and AHP (Fig. 4C4). Of 182 medullar 5-HT neurons, 31% of the neurons (57/182) did not show any significant change in RMP by muscarine (Fig. 4C1). Analysis of 57 5-HT neurons showed that muscarine did not induced any significant change in RMP (Fig. 4C5), rheobase (Fig. 4C6), AP height (Fig. 4C7), AHP depth (Fig. 4C8) and Rin (Fig. 4C9). Detailed data were presented in Supplementary Table 6. The above results showed that muscarine mimicked the varying effects of ACh on 5-HT neurons.

Similar to Fig. 3E, we marked the distribution of 5-HT neurons that were depolarized, hyperpolarized and unchanged by muscarine, respectively, in Fig. 4D. We further analyzed the relationship between the effects of muscarine and the location of PPR and MRN (Fig. 4D1). The neurons with membrane potential depolarization were concentrated more in PPR (72.5%, 87/120) than MRN (19.3%, 12/62), while neurons of membrane potential unchanged were mainly distributed in MRN (69.4%, 43/62,). The proportion of hyperpolarization neurons in PPR and MRN was 15.8% (19/120) and 11.3% (7/62), respectively (Fig. 4D2). These results showed that the PPR and MRN location dependence of muscarinic modulation of 5-TH neurons was similar to that of ACh on the 5-HT neurons. These location-related different responses to ACh and muscarine suggested that the PPR and MRN 5-HT neurons in medulla could play different functional roles in locomotion.

Based on the multi-nuclear organization of ventromedullary 5-HT neurons, we further examined the rostrocaudal distribution of mAChR-mediated modulatory effects on 5-HT neuronal excitability in this study. We divided the medullary slices into four consecutive sections along the rostrocaudal axis. Sections 1 and 2 were grouped as the rostral region, while sections 3 and 4 were grouped as the caudal region (Supplementary Fig. 3A). We then characterized the response profile (excitation, inhibition, no change) of identified 5-HT neurons to muscarine application within each of these regions (Supplementary Fig. 3B).

Analysis of the rostrocaudal distribution of muscarine responses revealed remarkably similar proportions of excited, inhibited, and unresponsive 5-HT neurons between rostral (sections 1 & 2; $n = 53$ neurons) and caudal (sections 3 & 4; $n = 34$ neurons) regions of the ventral medulla (Supplementary Fig. 3B, C). In the rostral region, muscarine receptor activation excited 25 neurons (25/53, 47%), inhibited 13 (13/53, 25%), and elicited no change in 15 (15/53, 28%). Similarly, in the caudal region, 16 neurons (16/34, 47%) were excited, 9 (9/34, 26.5%) were inhibited, and 9 (9/34, 26.5%) showed no response (Supplementary Fig. 3D). These results suggest that the modulatory effect of muscarine on 5-HT neuron excitability does not significantly differ along the rostrocaudal axis of the medulla.

M3 receptors mediated enhancement of excitability of 5-HT neurons

Of five receptor subtypes of mAChR (M1-M5), M1, M3, and M5 are preferentially coupled to Gq/11 and activate phospholipase C, which initiates the phosphatidylinositol trisphosphate cascade leading to increased neuronal excitability[44]. On the other hand, however, M2 and M4 are coupled to Gi/o, and inhibit adenylyl cyclase activity. They activate G protein-gated potassium channels, leading to hyperpolarization of the RMP and decreased neuronal excitability[44,45].

We first investigated the possible role of M1 muscarinic receptors in modulating excitability of 5-HT neurons by bath application of 10 μM telenzepine, the M1 receptor antagonist. The experiment results ($n = 8$) showed that blocking the M1 receptors did not affect the muscarine-depolarized membrane potential (Fig. 5A1, A5). As depicted in Fig. 5A, 20 μM muscarine depolarized the membrane potential (Fig. 5A1, A5) and reduced the rheobase (Fig. 5A2, A6), Rin (Fig. 5A3, A9), AP height (Fig. 5A4, A7), and AHP depth (Fig. 5A4, A8). These effects were not blocked by telenzepine (Fig. 5A5-A9), suggesting that M1 receptor was not involved in muscarinic modulation of 5-HT neurons in medulla. Detailed data were presented in Supplementary Table 7.

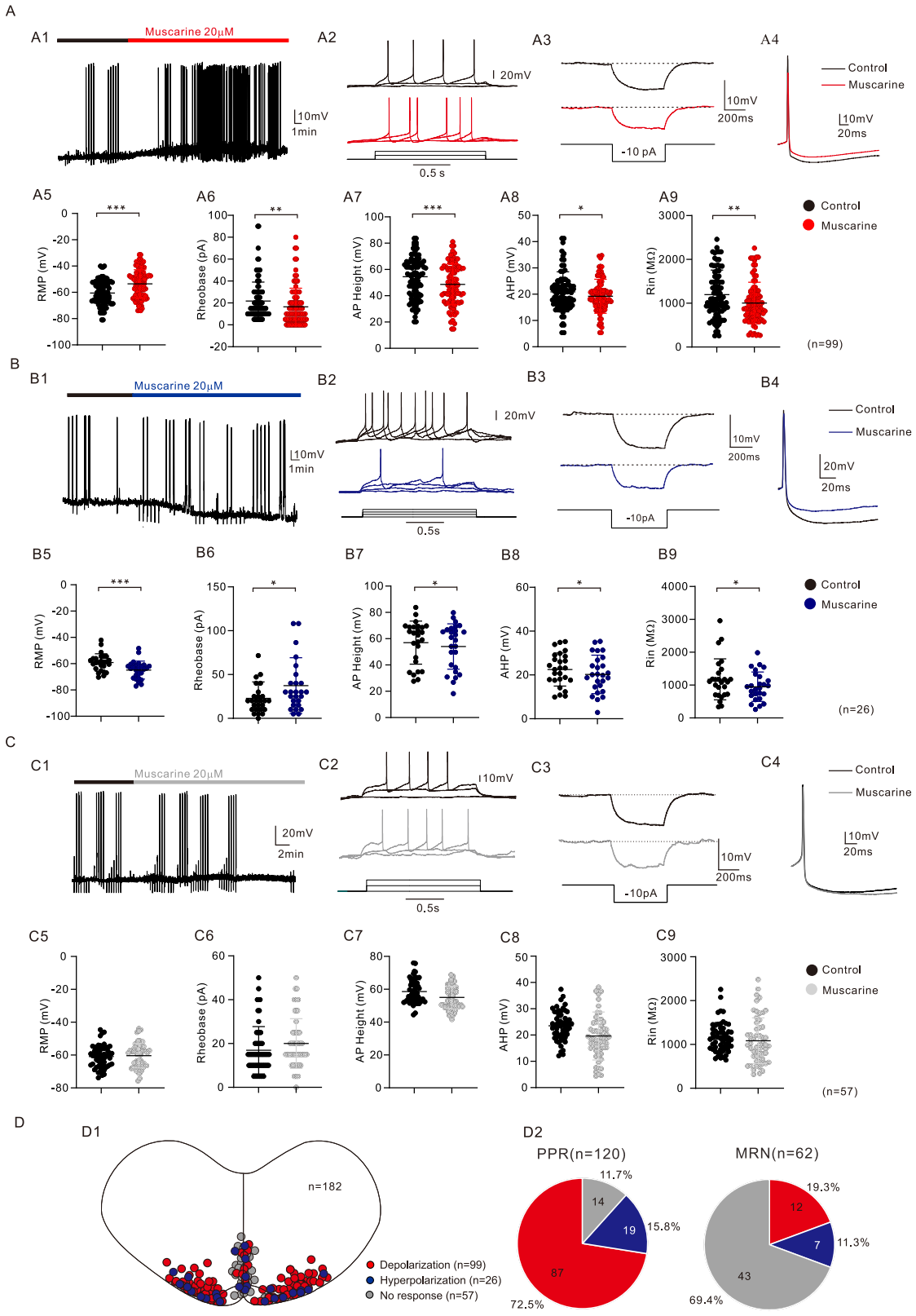

We further assessed the role of M3 receptors in modulating 5-HT neurons. Muscarine depolarized RMP and reduced rheobase, Rin, AP height and AHP depth (Fig. 5B1-B4, red traces) in this neuron. Bath application of 5 μM 4-DAMP, the M3 receptor antagonist, substantively removed the depolarization of RMP and reduction of rheobase, Rin, AP height and AHP depth (Fig. 5B1-B4, green traces), respectively. Statistical results from 16 neurons indicated that muscarine induced depolarization of RMP by 6.0 ± 2.5 mV (Fig. 5A5, red circles) and reduction of rheobase, (Fig. 5A6, red circles), AP height (Fig. 5C7, red circles), AHP depth (Fig. 5C8, red circles) and Rin (Fig. 5C9, red circles) by 5.9 ± 3.2 pA, 7.2 ± 3.4 mV, 3.2 ± 1.9 mV, and 176.2 ± 110.9 MΩ, respectively. 4-DAMP significantly blocked the muscarine-induced depolarization of RMP and

Fig. 4 | The modulation of muscarine on 5-HT neurons excitability. A Muscarine increased the excitability of 5-HT neurons. **A1** Muscarine induced membrane potential depolarization and spontaneous firing. **A2** Muscarine decreased the rheobase. **A3** Muscarine reduced the Rin. **A4** Superimposed action potential recorded from a 5-HT neuron before (black) and after muscarine (red) showed that muscarine decreased AP height and AHP. **A5-A9** Statistical results for the RMP, Rheobase, AP height AHP depth and Rin of 5-HT neurons recorded in control (black) and in the presence of 20 μM muscarine (red). **B** Muscarine decreased the excitability of 5-HT neurons. **B1** Muscarine induced membrane potential hyperpolarization. **B2** Muscarine increased the rheobase. **B3** Muscarine reduced the Rin. **B4** Superimposed action potential recorded from a 5-HT neuron before (black) and after muscarine (blue), muscarine decreased AP height and AHP. **B5-B9** Statistical results listed for the RMP, Rheobase, AP height AHP depth and Rin of 5-HT neurons recorded in control (black) and in the presence of 20 μM muscarine (blue). **C** Muscarine did not significantly change the excitability of 5-HT neurons. **C1-C2** Muscarine did not statistically change RMP (**C1**) and rheobase (**C2**). **C3** Muscarine reduced the Rin. **C4** Superimposed action potential recorded from a 5-HT neuron before (black) and after muscarine (grey), muscarine did not substantively change AP height and AHP. **C5-C9** Statistical results summarized for the RMP, Rheobase, AP height AHP depth and Rin of 5-HT neurons recorded in control (black) and in the presence of 20 μM muscarine (grey). **D** Muscarine effects on 5-HT neuron RMP in the medulla. **D1** Three-type effects induced by muscarine on the RMP of 5-HT neurons and their distribution. **D2** Proportions of three type effects by muscarine on the RMP in PPR and MRN, respectively. Error bars represented SD; paired t-test performed; ∗: $P < 0.05$, ∗∗: $P < 0.01$, ∗∗∗: $P < 0.001$.

reduction of rheobase, AP height, AHP depth, and Rin (Fig. 5B5-9, green circles). Detailed data were presented in Supplementary Table 8. These results suggested that M3 receptors mediated the muscarine-increased excitability of 5-HT neurons in medulla.

Finally, we investigated the effect of M5 muscarinic receptors on the excitability of 5-HT neurons. Similarly, 20 μM muscarine depolarized RMP (Fig. 5C1) and reduced rheobase, Rin, AP height and AHP depth in a medullar 5-HT neuron (Fig. 5C2-C4, red traces). Bath administration of 5 μM VU6008667, the M5 receptor inhibitor, did not restore the muscarine-induced depolarization of the membrane potential (Fig. 5C1) and reduction of rheobase (Fig. 5C2, green trace), Rin (Fig. 5C3, green trace), AP height and AHP depth (Fig. 5C4, green trace). Statistic results (n = 8) indicated that muscarine significantly depolarized RMP by 8.2 ± 2.5 mV (Fig. 5C5, red circles) and lowered rheobase (Fig. 5C6, red circles), AP height (Fig. 5C7, red circles), AHP depth (Fig. 5C8, red circles), and Rin (Fig. 5C9, red circles) by 9.4 ± 5.3 pA, 5.6 ± 2.3 mV, 2.8 ± 1.6 mV, and 244.7 ± 123.7 MΩ, respectively. These muscarine-induced changes in membrane properties were not antagonized by VU6008667 (Fig. 5C5-C9, green circles), suggesting that the M5 receptors were not involved the muscarine-increased excitability of 5-HT neurons in medulla. See Supplementary Table 9 for detailed data.

M2 and M4 receptors co-mediated the decreased excitability of 5-HT neurons

It has been shown that activation of M2 and M4 receptors hyperpolarizes the RMP and reduces neuronal excitability in the pedunculopontine tegmental nucleus, which mediates respiratory modulation in rats[44,46]. In this study, we explored the possible roles of M2 and M4 receptors in regulating excitability of medullar 5-HT neurons. Figure 6A was an example for M2 receptors, where 20 μM muscarine induced a hyperpolarization of RMP (Fig. 6A1), accompanied with an increase in rheobase (Fig. 6A2, blue traces) and a decrease in Rin (Fig. 6A3 blue traces), AHP depth and AP height (Fig. 6A4 blue traces), respectively. Bath application of 5 μM methoctramine, the M2 receptor antagonist, significantly removed the muscarine-induced inhibitory effects on this neuron (Fig. 6A1-A4, orange traces). Statistical results from 10 neurons indicated that muscarine hyperpolarized RMP by 6.8 ± 1.8 mV (Fig. 6A5, blue circles), increased rheobase (Fig. 6A6, blue circles), and reduced AP height (Fig. 6A7, blue circles), AHP depth (Fig. 6A8, blue circles) and Rin (Fig. 6A9, blue circles) by 15 ± 10.2 pA, 4.7 ± 1.7 mV, 4.8 ± 2.5 mV and 300.7 ± 127.1 MΩ, respectively. Methoctramine significantly antagonized the muscarinic effects on the RMP, rheobase, AP height, AHP depth and Rin (Fig. 6A5-A9, orange circles). See Supplementary Table 10 for detailed data. These results suggested that M2 receptors mediated the muscarine-induced lowering of excitability of 5-HT neurons in medulla.

Next, we investigated M4 receptors in modulating excitability of 5-HT neurons. Similarly, 20 μM muscarine hyperpolarized the RMP, increased rheobase, and reduced AP height, AHP depth, and Rin, respectively, in a medullar 5-HT neuron (Fig. 6B1-B4, blue traces). Administration of 10 μM tropicamide, the M4 receptor antagonist, completely removed the muscarine-induced inhibitory effects on this neuron (Fig. 6B1-B4, green traces). Statistic results ($n = 9$) showed that muscarine induced a hyperpolarization of RMP by 5.3 ± 1.7 mV (Fig. 6B5, blue circles), increase of rheobase by 10 ± 3.3 pA, (Fig. 6B6, blue circles), and reduction of AP height (Fig. 6B7, blue circles), AHP depth (Fig. 6B8, blue circles) and Rin (Fig. 6B9, blue circles) by 6.3 ± 3.2 mV, 3.7 ± 1.7 mV, and 249.1 ± 85.7 MΩ, respectively. Tropicamide significantly removed the muscarine-induced changes in 5-HT neurons (Fig. 6B5-B9, green circles). See Supplementary Table 11 for detailed data. These results implicated that muscarine-induced decreased excitability of 5-HT neurons was also mediated by activation of M4 receptors.

Our data confirmed that both M2 and M4 receptors were involved in mediating decreased neuronal excitability of 5-HT neurons in medulla. We next investigated the interaction between these two receptors and determined which one dominated muscarinic modulation of 5-HT neurons. An example was shown in Fig. 6C1, where a 20 μM muscarine hyperpolarized the membrane potential by 5.9 mV in average, accompanied with an increase in rheobase (15 pA) and a decrease in AP height (5 mV), AHP depth (3.2 mV) and Rin (341 MΩ). Bath application of 5 μM methoctramine failed to block muscarinic effects on this neuron. We then further applied 10 μM tropicamide to the recording solution in the presence of muscarine and methoctramine. Tropicamide completely removed muscarine-induced hyperpolarization of RMP in this neuron, suggesting that the muscarine-induced decreased excitability was mainly mediated by M4 receptors in this 5-HT neuron. Figure 6C2 indicated that overlapping blockade of M4 receptor restored muscarinic-induced reduction in neuronal excitability (RMP, rheobase, AP height, AHP and Rin) when M2 receptor function was not fully removed (Fig. 6C2).

In a subset of 5-HT neurons, the M2 receptor was primarily responsible for the inhibitory effect of acetylcholine. An example was shown in Fig. 6D1. Similarly, 20 μM muscarine hyperpolarized the RMP in this neuron with an increase in rheobase and a decrease in Rin, AP height and AHP depth, respectively. Bath administration of 10 μM tropicamide did not abolish the muscarine-induced inhibitory effects on this neuron. However, 5 μM methoctramine significantly antagonized the muscarinic effects on this neuron, implicating that M2 receptors played a dominant role in regulating the excitability of this 5-HT neuron. The experiment data showed that additive blockade of M2 receptors antagonized muscarinic-induced reduction in neuronal excitability when M4 receptors were not completely blocked (Fig. 6D2). These results suggested that both M2 and M4 receptors mediated the decreased excitability of 5-HT neurons. In some neurons, however, they could complement each other to complete this function.

Expression of M2, M3 and M4 receptors in medullar 5-HT neurons

The above experiments results suggested that M3 receptors mediated the muscarine-increased excitability of medullar 5-HT neurons and that M2 and M4 receptors contributed to the muscarine-decreased excitability of the neurons, whereas M1 and M5 receptors were not involved in the muscarinic modulation of 5-HT neurons. Given the absence of glutamatergic and GABAergic synaptic transmission blockers, the observed effects of ACh/

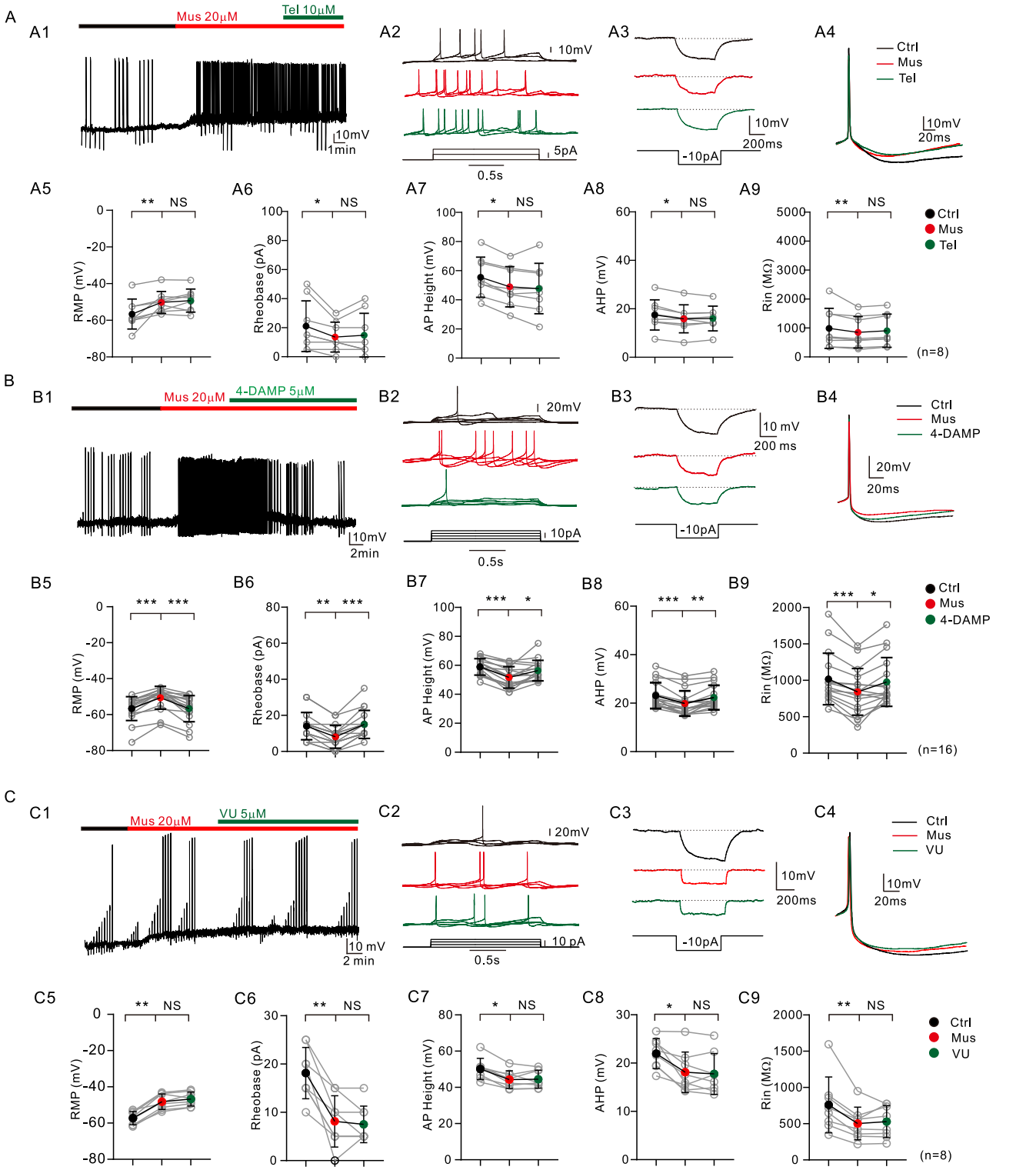

Fig. 5 | The mAChR-M3 receptors mediated the muscarine-induced excitatory effect on medullar 5-HT neurons. A M1 receptor was not involved the modulation of muscarine on 5-HT neurons. **A1** Muscarine-mediated depolarization and spontaneous firing persisted following application of M1 receptor antagonist telenzepine (10 μM). Telenzepine did not change the effect of the muscarine on rheobase (**A2**), Rin (**A3**), AP height and AHP depth (**A4**). **A5-A9** Statistical results listed for the RMP, Rheobase, AP height AHP depth and Rin of 5-HT neurons recorded in control (black), 20 μM muscarine (red) and 10 μM telenzepine (green). **B** M3 receptor was involved the modulation of muscarine on 5-HT neurons. **B1** Muscarine-mediated RMP depolarization and spontaneous firing were blocked by 4-DAMP (5 μM), M3 receptor antagonist. 4-DAMP removed the muscarine-induced decrease in rheobase (**B2**), Rin (**B3**), AP height, and AHP depth (**B4**). **B5-B9** Statistical results showed for the RMP, Rheobase, AP height AHP depth and Rin of 5-HT neurons recorded in control (black), 20 μM muscarine (red) and 5 μM 4-DAMP (green), respectively. **C** M5 receptor was not involved in muscarinic modulation of 5-HT neurons. **C1** Muscarine-mediated depolarization persisted following application of 5 μM VU 6008667, M5 inhibitor. VU 6008667 did not alter the effect of muscarine on rheobase (**C2**), Rin (**C3**), AP height and AHP depth (**C4**). **C5-C9** Statistical results for the RMP, Rheobase, AP height AHP depth and Rin of 5-HT neurons recorded in control (black), 20 μM muscarine (red) and 5 μM VU 6008667 (green), respectively. Mus muscarine, Tel Telenzepine, VU VU 6008667. Error bars represented SD; one-way ANOVA performed, ∗:$P < 0.05$, ∗∗: $P < 0.01$, ∗∗∗: $P < 0.001$, NS: no significant difference.

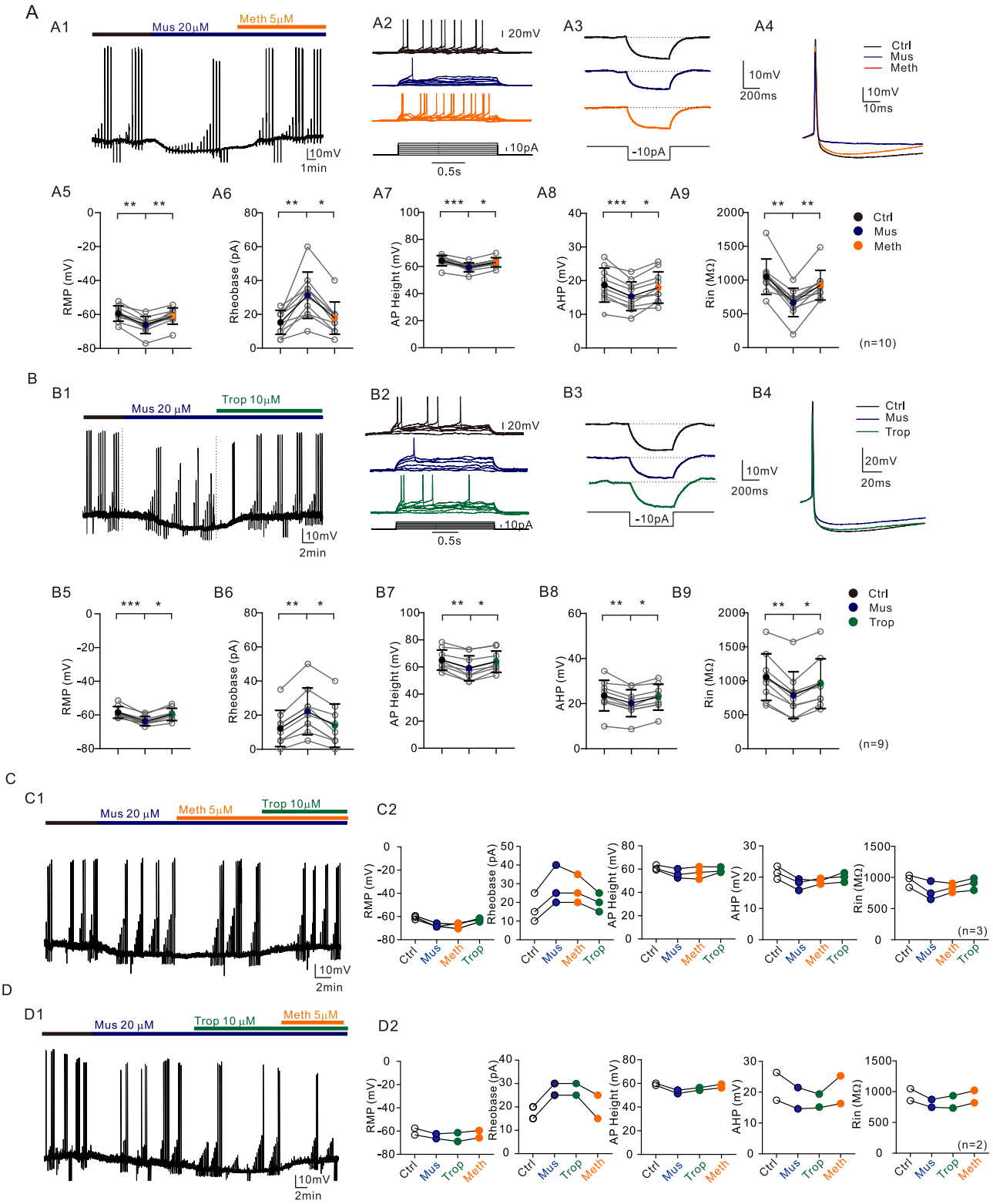

muscarine on 5-HT neuron excitability may involve both direct actions and indirect modulation via local microcircuits. To verify that acetylcholine acts directly on medullary 5-HT neurons, in the following experiments we examined the expression of mAChRs on the 5-HT neurons in the medulla. To this end, the immunofluorescent staining was undertaken for the mAChRs subtypes 2-4 in medullar 5-HT neurons. Experimental results clearly showed that M2 (Fig. 7A1), M3 (Fig. 7A2) and M4 (Fig. 7A3) receptors (red) were expressed on the *ePet-EYFP* positive 5-HT neurons (green) in medulla. In the present study, our electrophysiological data demonstrated that M2 and M4 receptors co-mediate the muscarine-induced reduction in neuronal excitability in a subset of 5-HT neurons. Accordingly, we further confirmed, via immuno-co-expression analysis, that M2 and M4 receptors were co-expressed on the membrane of 5-HT neurons in medulla (Fig. 7A4). The immunofluorescent results supported the involvement of mAChRs subtypes 2-4 in mediating the muscarinic modulation of 5-HT neurons.

Fig. 6 | The mAChR M2 and M4 receptors mediated the muscarine-induced inhibitory effect on medullar 5-HT neurons. **A** M2 receptor was involved the modulation of muscarine on 5-HT neurons. **A1** Muscarine-mediated RMP hyperpolarization were blocked by methoctramine, M2 receptor antagonist. Methoctramine (5 μM) blocked the effect of muscarine-induced increase in rheobase (**A2**) and decrease in Rin (**A3**), AP height, and AHP depth (**A4**). **A5-A9** Statistical results summarized for the RMP, Rheobase, AP height, AHP depth and Rin of 5-HT neurons recorded in control (black), 20 μM muscarine (blue) and 5 μM methoctramine (orange). **B** M4 receptor mediated muscarinic modulation of 5-HT neurons. **B1** Muscarine-induced RMP hyperpolarization were blocked by 10 μM tropicamide, M4 receptor antagonist. Tropicamide blocked the effect of muscarine-induced increase in rheobase (**B2**), and decrease in Rin (**B3**), AP height, AHP depth (**B4**). **B5-B9** Statistical results shown for the RMP, Rheobase, AP height AHP depth and Rin of 5-HT neurons in control (black), 20 μM muscarine (blue) and 10 μM tropicamide (green), respectively. **C**, **D** The coupling effects of M2 and M4 receptors on 5-HT neurons. **C1** Muscarine-induced hyperpolarization was not blocked by M2 antagonist methoctramine, but was completely removed by M4 antagonist tropicamide. **C2** The RMP, Rheobase, AP height, AHP depth and Rin of three 5-HT neurons were recorded in control (black), 20 μM muscarine (blue), 5 μM methoctramine (orange) and 10 μM tropicamide (green), respectively. **D1** Muscarine-induced hyperpolarization was not blocked by M4 antagonist tropicamide, but was blocked by M2 antagonist methoctramine. **D2** The RMP, Rheobase, AP height, AHP depth and Rin of two 5-HT neurons were recorded in control (black), 20 μM muscarine (blue), 10 μM tropicamide (green) and 5 μM methoctramine (orange), respectively. Mus muscarine, Meth methoctramine, Trop tropicamide. Error bars represented SD; one-way ANOVA performed, ∗: $P < 0.05$, ∗∗: $P < 0.01$, ∗∗∗: $P < 0.001$.

Projection of cholinergic neurons in MLR to the ventral medulla

The medullary reticular formation relays MLR inputs during locomotion, and previous studies have confirmed that a large number of neurons in the MLR project to the medulla[5,47]. Therefore, we hypothesized that cholinergic neurons in the MLR projected to the medullary 5-HT neurons and modulated their excitability. To test this hypothesis, we crossed *ChAT-IRES-Cre* mice with the *R26-stop-EYFP* conditional reporter line to permanently label cholinergic neurons (Fig. 7B1). We then retrogradely labeled *Chat-EYFP* positive neurons to detect the projection of cholinergic neurons to the MLR area (Fig. 7B). A retrograde tracer dextran tetramethylrhodamine was injected into the ventral medullary reticular formation of transgenic *ChAT-IRES-EYFP* mice of P3-P6 (Fig. 7B2, see "Methods"). We then identified the cholinergic neurons from retrogradely labeled neurons in pedunculopontine nucleus (PPN) and the cuneiform nucleus (CnF). As shown in Fig. 7C, the *Chat-EYFP* positive neurons were visualized in PPN but not CnF. However, neurons in both PPN and CnF were retrogradely labeled, suggesting that the MLR neurons, either cholinergic or non-cholinergic, projected to the ventral medulla. The results suggested the possible existence of a neural pathway through which PPN cholinergic neurons could modulate the medullary 5-HT neurons.

Fictive locomotion regulated by medullary muscarinic modulation

The locomotor command originates in the mesencephalic locomotor region (MLR), which projects to spinal locomotor circuits through descending pathway of RSNs in the pons and medulla[1,2,27]. Previous studies reported that cholinergic neurons in the MLR played an essential role in regulating rhythmic activities and locomotor output by activating medullary neurons through mAChRs in lamprey[48,49]. However, it is unclear which mAChRs are involved in this modulating process. Based on the results from this study, we investigated the effects of activating mAChRs of medulla on the rhythmic generation and locomotor activities. Fictive locomotion was initiated by bath application of 5-HT (20–30 μM) and NMDA (3–5 μM) to the spinal cord compartment, with concurrent perfusion of muscarine (20 μM) to the medullary compartment. During mAChR blockade experiments, subtype-specific antagonists were co-applied with the sustained muscarine background to the medulla while preserving spinal neurochemistry. Ventral root recordings were collected via suction glass electrodes attached to the left and right fifth lumbar ventral roots (lL5 and rL5) of the spinal cord (Fig. 8A).

Experiment results showed that methoctramine (2 μM), the M2 receptor antagonist, promoted the locomotor activities and increased the cycle frequency (Fig. 8B1, B3) with little change in the coordination and ENG amplitude of locomotion (Fig. 8B2, B4). In contrast, the M3 receptors exhibited a big effect on the fictive locomotion. 5 μM 4-DAMP abolished the rhythmic activities and removed left-right coordination of fictive locomotion (Fig. 8C1, C2). Statistical results from 9 mice indicated that 4-DAMP significantly reduced the cycle frequency and ENG amplitude (Fig. 8C3, C4). Similar to the results of M2 receptors, blockage of M4 receptors by tropicamide (5 μM) significantly increased the cycle frequency (Fig. 8D1, D3) with no substantial change in step coordination and ENG amplitude (Fig. 8D2, D4). Detailed data were presented in Supplementary Table 12. In this study, we also examined the role of medullary M1 and M5 acetylcholine receptors in regulating fictive locomotion. Blockade of M1 receptors with telenzepine or M5 receptors with VU 6006887 did not affect fictive locomotion (please see Supplementary Fig. 4). The above results suggested that activation of M2 and M4 receptors in medulla slowed down the cycle frequency without changing the strength of locomotor output, while activation of M3 receptors increased the cycle frequency as well as the left-right coordination.

Verification of muscarinic modulation of fictive locomotion with modeling

5-HT neurons located in the medulla play an important role in initiating locomotion[14,15]. Both our electrophysiological and immunohistochemistry studies have confirmed the expression of mAChRs (M2-M4) in medullar 5-HT neurons. Based on these results we built a simplified spinal network[50], which could generate rhythmic activities similar to fictive locomotion as recoded in our experiments (Fig. 8). The CPG network was driven by excitatory input from medullar 5-HT neurons which received excitatory and inhibitory inputs mimicked by activating M3 and M2/M4 receptors, respectively (Fig. 9A1). Simulation results showed that activation of medullary 5-HT neurons initiated rhythmic bursting of left and right half-centers, with a cycle frequency of 0.3 ± 0.03 Hz (Fig. 9A2).

In the model experiments, we simulated the results of whole spinal ventral root recording experiments by selectively reducing the excitatory and inhibitory synaptic conductances, which corresponded to the antagonist effects of M3 and M2/M4 receptors, respectively, on the 5-HT neurons. When the excitatory synaptic conductance was decreased to 25% of control levels, the rhythm of fictive locomotion was disrupted, with the average stepping frequency declining to 0.16 ± 0.06 Hz (Fig. 9B1). In contrast, reduction of inhibitory synaptic conductance to 25% resulted in a significant enhancement of cycle frequency to 0.38 ± 0.03 Hz (Fig. 9B2). These results were consistent with our experimental observations in whole spinal ventral root recording studies.

To further confirm the modulatory role of excitatory and inhibitory synapses on medullary 5-HT neurons in regulating fictive locomotion rhythms, we systematically increased excitatory and inhibitory synaptic conductances. Simulation results demonstrated that increasing the conductance of excitatory synapses to 200% (mimicking the enhancement of M3 receptor activation in 5-HT neurons) increased cycle frequency between the left and right half-centers (0.33 ± 0.04 Hz; Fig. 9C1). Conversely, increasing inhibitory synaptic conductance to 200% (simulating enhanced activation of M2/M4 receptors) reduced the cycle frequency to 0.23 ± 0.02 Hz (Fig. 9C2). These results aligned with experimental data and confirmed distinct functional roles of mAChR subtypes (M2, M3, and M4) of medullary 5-HT neurons in modulating locomotion.

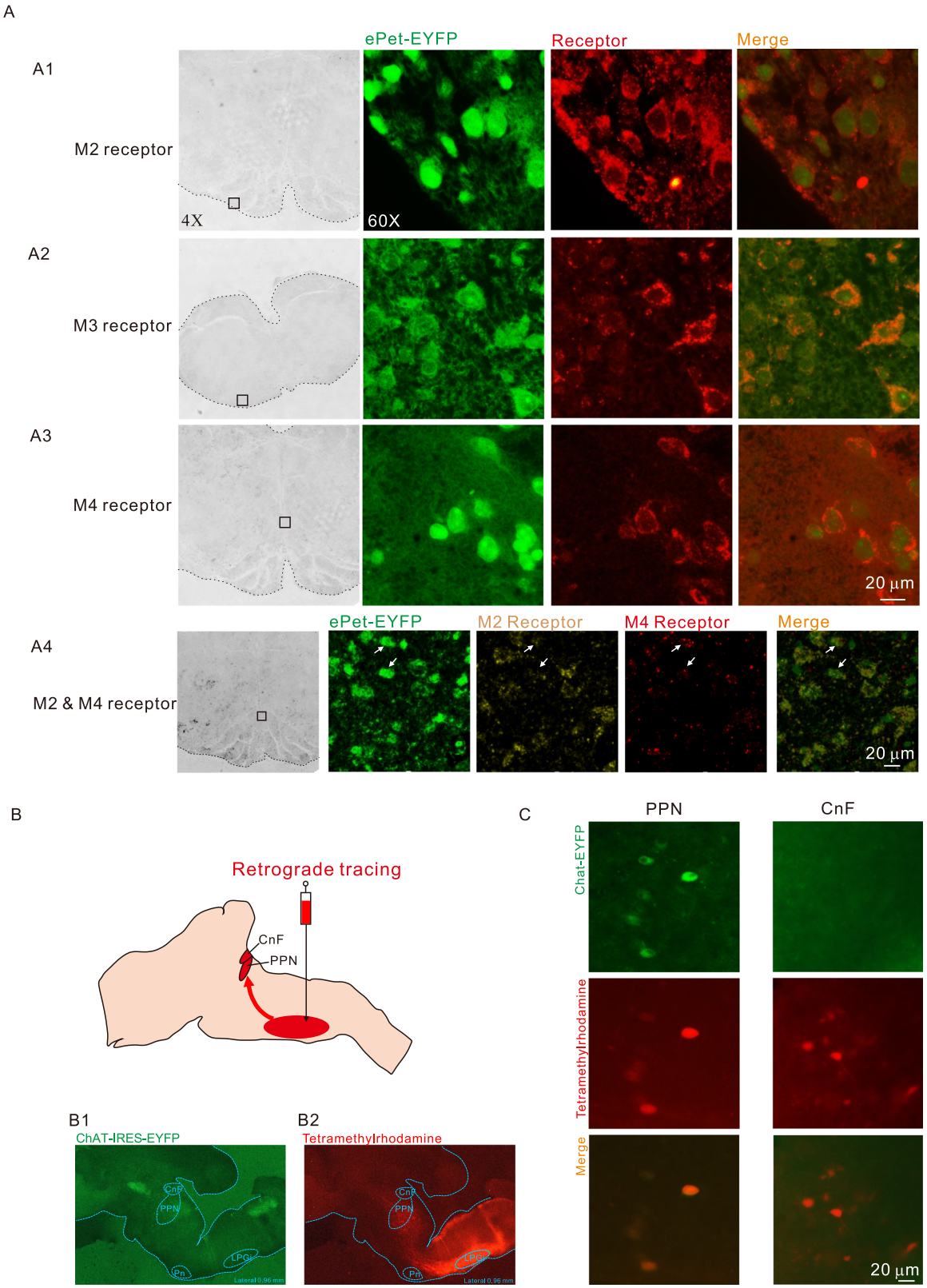

Fig. 7 | Images from immunofluorescence and retrograde labeling experiments. **A** Localization of M2 (**A1**), M3 (**A2**), and M4 (**A3**) receptors in the medulla. The first column contained images of a representative transverse medulla section, demonstrating the position of the view within the black box. The next three columns contained images of 5-HT neurons (green), receptors (red), and the merged images (yellow). **A4** Colocalization of M2 and M4 receptor subtypes within identified 5-HT neurons in the ventral medulla. **B** Injection of a retrograde tracer, dextran tetramethylrhodamine (TMRM 25%), into the ventral medulla. Distribution of cholinergic neuronal clusters in sagittal brainstem sections of transgenic mice (Chat-IRES-EYFP), with green fluorescence indicating cholinergic neurons (**B1**). Distribution of tetramethylrhodamine in the sagittal brainstem (**B2**). CnF: cuneiform uncleus; PPN pedunculopontine nucleus, Pn pontine nuclei, LPGi lateral paragigantocellular nucleus. **C** Examples of fluorescence staining of cholinergic neurons (green) with retrograde labeling (red) in the pedunculopontine nucleus (PPN). Noncholinergic neurons of the cuneiform nucleus (CnF) were also fluorescently labeled.

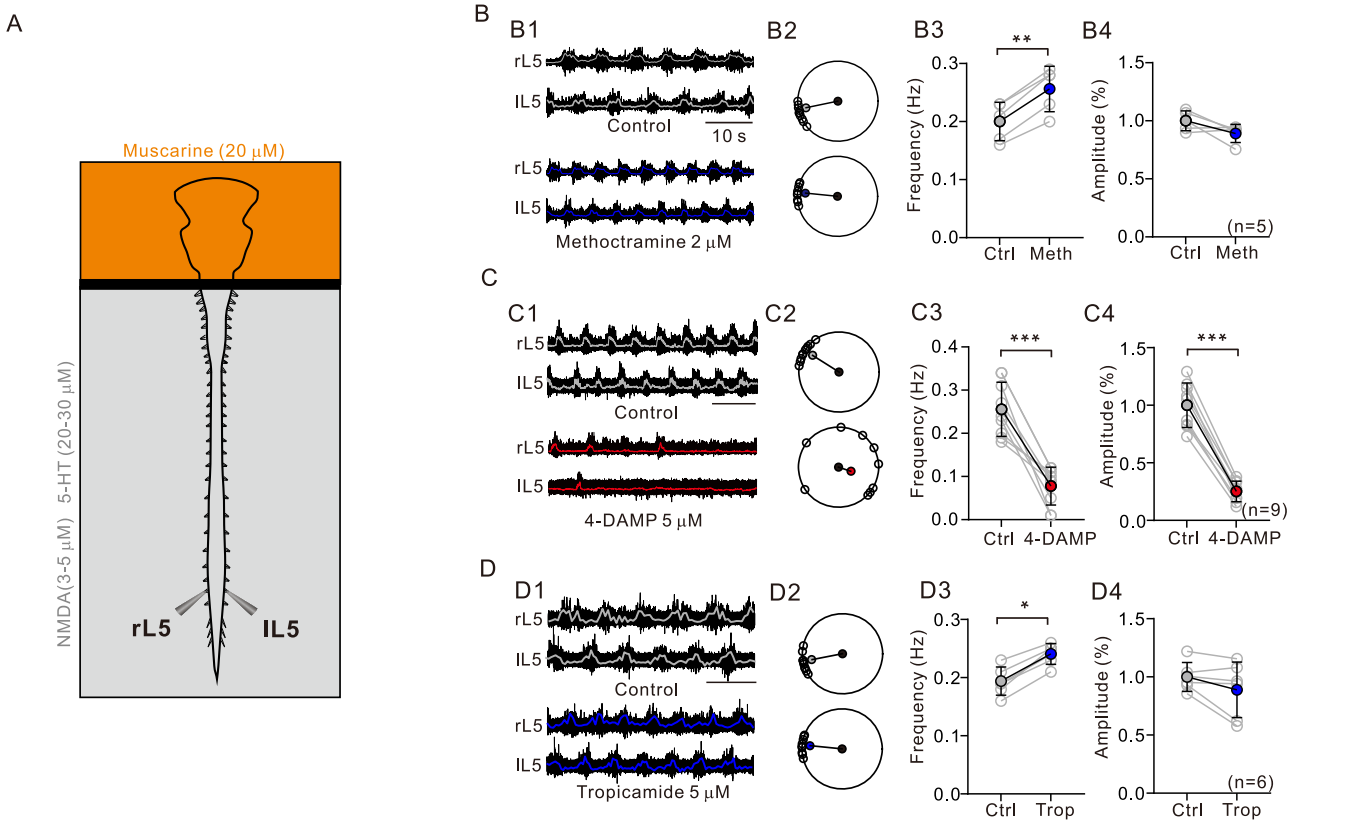

Fig. 8 | The role of medullary muscarinic receptors in regulating fictive locomotion. A Schematic representation of the whole spinal cord ENG recording with glass electrodes from the lumbar segment L5 (both right and left). Vaseline (black line) was used to divide the medulla (yellow area) and spinal cord (grey area) in the cervical region. 5-HT and NMDA were applied to the spinal cord area and muscarine were applied to medulla area. Ventral root recordings were recorded before and after bath application of methoctramine (**B**), 4-DAMP (**C**), and tropicamide (**D**) in the medulla, respectively. **B1**, **C1**, **D1** ENG activity recorded from the right and left L5 ventral roots during fictive locomotion, pre- and post-drug application. **B2**, **C2**, **D2** Polar plots represented the fictive locomotion pre- and post-drug application. Changes in frequency of step cycles (**B3**, **C3**, **D3**) and amplitude of ENG (**B4**, **C4**, **D4**) before and after drug administration during fictive locomotion. Analyzed by paired-sample t-tests, error bars represented SD; ∗: $P < 0.05$, ∗∗: $P < 0.01$, ∗∗∗: $P < 0.001$.

Discussion

This study elucidates cholinergic regulation of medullary 5-HT neurons and their role in fictive locomotion. Electrophysiological and immunohistochemical evidence identified M2/M3/M4 receptor involvement, with functional assays showing M2/M4 blockade increases step frequency, while M3 inhibition abolishes locomotion. Retrograde tracing revealed an MLR-to-medulla cholinergic pathway, and computational modeling demonstrated receptor-specific modulation of locomotor rhythm, speed, and stability. These findings establish a medullary pathway where M2/M3/M4 coordination controls locomotion (Fig. 10).

Activation of mAChRs regulated neuronal excitability

In mammals, mAChRs mediate most metabotropic actions of ACh in the central nervous system (CNS)[44,51]. mAChRs are coupled either to Gq/11 proteins (M1, M3, and M5 subtypes) that activate phospholipase C or Gi/o proteins (M2 and M4 subtypes) that negatively couple to adenylate cyclase[52], linking ACh activity to a variety of biochemical signaling cascades. In the present study, we found that activating mAChRs led to two opposite effects on 5-HT neurons, i.e. increased as well as decreased neuronal excitability in terms of changes in RMP and rheobase. These findings are generally consistent with previous studies indicating that M3 receptors contribute to the muscarine-induced increased neuronal excitability and M2 and M4 receptors mediate the muscarine-induced decreased neuronal excitability[35,44]. M1 and M5 receptors did not mediate the cholinergic effect on 5-HT neurons. In fact, similar results were also observed in our recent study in persistent inward currents (PICs), where activation of M3 receptors enhanced PICs in 5-HT neurons, whereas M1 and M5 receptors were not involved in this process[20].

In this study, there was always a decrease in Rin, AHP depth and AP height no matter whether muscarine induced an increase or decrease in RMP of 5-HT neurons (Fig. 4). However, different results have been reported in spinal motoneurons of neonatal mice. Activating the M2 receptors induced a decrease in Rin and AHP depth, whereas activating the M3 receptors caused an increase in Rin[35]. The different results could be due to different types and properties between medullar 5-HT neurons and spinal motoneurons. Although muscarine induced varying effects on 5-HT neurons, modulation of rheobase was functionally consistent. Our data showed that an increase in RMP was always accompanied by a decreased rheobase which increased neuronal excitability, while the decreased RMP occurred with an increased rheobase which reduced neuronal excitability. These results suggested that mAChRs-mediated modulation of rheobase could play a dominant role in cholinergic-regulating excitability of 5-HT neurons.

It must be acknowledged that experiments involving synaptic blockers were not conducted in the present study. As a result, we cannot rule out potential indirect effects mediated by other neurotransmitters that might be excited or inhibited by acetylcholine or muscarine. Nevertheless, this study revealed a predominant excitatory influence of M3 receptor activation, along with inhibitory effects mediated by M2/M4 receptors, on 5-HT neurons. By contrast, no significant effects were observed for M1 or M5 receptors—which have been reported to exert excitatory actions in other neuronal types[53]—under the current

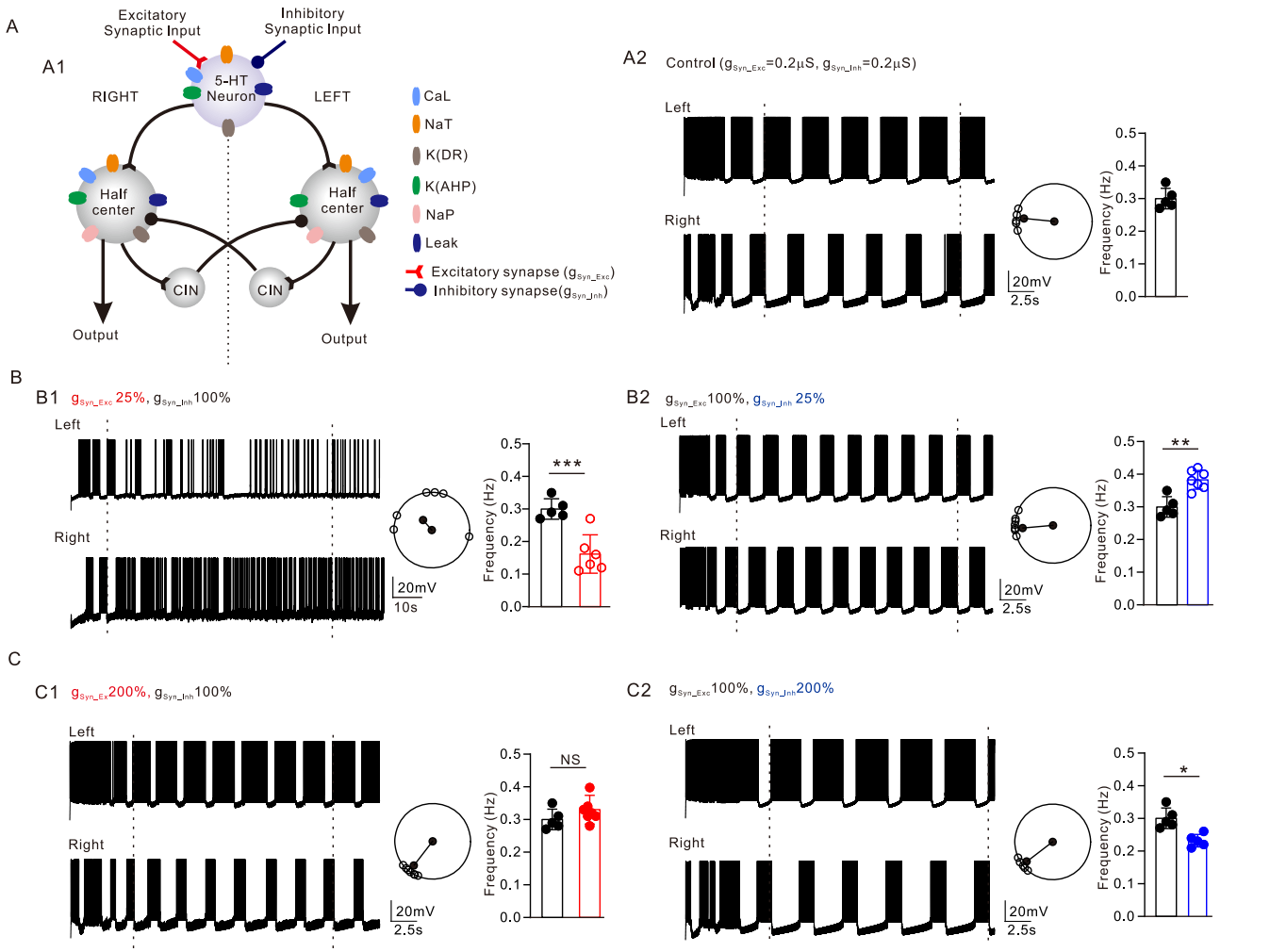

Fig. 9 | Modeling study of rhythmic generation with network of central pattern generator (CPG). A CPG model with rhythmic generation. **A1** The CPG model was composed of left and right half-center pools, coupled by reciprocal inhibition of commissural interneuron pools (CIN), and driven by cholinergic inputs from the medullar 5-HT neuron pool. This panel was hand-drawn by us. **A2** Rhythmic activities of left and right half-centers were generated by excitatory (M3 receptor) and inhibitory (M2&M4) synaptic inputs to 5-HT neuron pool. g_{sye_Exc} = 0.2 μS and g_{sye_Inh} = 0.2 μS were set as control values. Polar plots described coordination of locomotion. The cycle frequency was measured as 0.3 ± 0.03 Hz. **B** Effect of reducing synaptic conductance on rhythmic activities. **B1** Reducing excitatory synaptic conductance gsye_Exc to 25% decreased rhythmic frequency to 0.16 ± 0.06 Hz and disrupted locomotion. **B2** Reducing inhibitory synaptic conductance g_{sye_Inh} to 25% increased the rhythmic frequency to 0.38 ± 0.03 Hz with preserved gait stability. **C** Effect of increasing synaptic conductance on rhythmic activities. **C1** Increasing g_{sye_Exc} to 200% increased the rhythmic frequency to 0.33 ± 0.04 Hz with stable gait. **C2** Increasing g_{sye_Inh} to 200% reduced rhythmic frequency to 0.23 ± 0.02 Hz with stable gait. Error bars represented SD; paired t-test performed; ∗: $P < 0.05$; ∗∗: $P < 0.01$,∗∗∗: $P < 0.001$, NS: no significant difference. Dash lines in rhythmic bursting represented boundaries within which the recordings were used to calculate frequency of step cycle and polar plots.

experimental conditions. Moreover, these findings from slice experiments were consistent with the ENG recordings of fictive locomotion-like activities in the isolated whole spinal cord (Fig. 8). Collectively, these results imply that M3 and M2/M4 receptors play dominant roles in modulating 5-HT neuronal excitability and fictive locomotion and integrating multi-pathway with cholinergic-serotonergic circuits serving as principal but not exclusive mediators. Further studies are required to address this issue in the future.

We also note that specific experiments blocking M3 receptors in the context of ACh-induced hyperpolarization, or M2/M4 receptors during ACh-induced depolarization, were not performed. In this study, receptor antagonists for M1–M5 were applied based on the canonical regulatory profiles of muscarinic receptors, namely, that M1, M3, and M5 typically mediate excitatory effects, while M2 and M4 mediate inhibitory effects on neuronal excitability[54]. This rationale underpinned our sequential application of M2 (or M4) and subsequently M4 (or M2) antagonists in cases where muscarine-induced hyperpolarization was not fully reversed by a single antagonist (Fig. 6C, D).

The distribution of the mAChRs in the central nervous system

Immunocytochemical and immunoprecipitation studies have revealed that the M1 receptors are widely distributed in the CNS of mammals[55]. M2 receptors are enriched in the brainstem, thalamus, cerebral cortex, hippocampus and striatum, and M3 receptors are widely expressed in both central and peripheral nervous systems[55]. M4 mAChRs are found in many brain regions, however they are most concentrated in the striatum, where they regulate dopamine release for normal basal ganglia function[56]. Relatively less is known about the M5 mAChR subtype, which represents less than 2% of the total CNS mAChR population[57]. In this study, we confirmed that M2, M3 and M4 receptors were expressed on medullar 5-HT neurons in *ePet-EYFP* mice (Fig. 7A). Our immunofluorescent data provided anatomic evidence for muscarinic-modulation of medullar 5-HT neurons. Also, our data were consistent with the Allen Mouse Brain Atlas (2009) developed by the Allen Institute for Brain Science available online at http://mouse.brain-map.org.

Our data demonstrated that M2 and M4 receptors were co-expressed on a subset of medullary 5-HT neurons (Fig. 7A4), providing anatomical

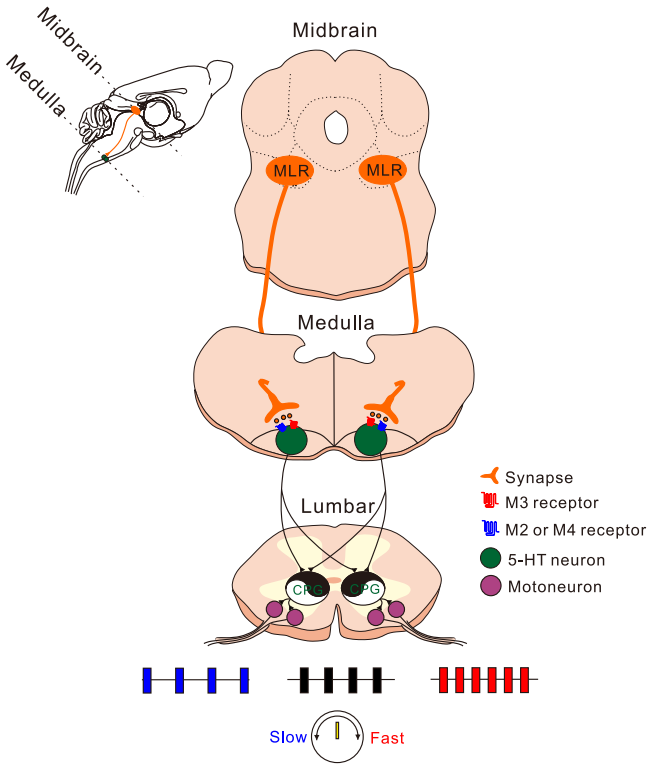

Fig. 10 | Functional roles of cholinergic pathway from MLR to spinal cord in generating locomotion. Release of acetylcholine from MLR to medullar area activates M2&M4 receptors, reduces excitability of medullar 5-HT neurons, and slows down locomotor frequency. Acetylcholine from MLR activates M3 receptors, increases excitability of medullar 5-HT neurons, and accelerates locomotor frequency. This Figure was hand-drawn by us.

support for their functional interaction. Electrophysiological results indicated that in the majority of 5-HT neurons, blockade of either M2 (77%, 10/13) or M4 receptors (82%, 9/11) alone was sufficient to abolish muscarine-induced inhibition (Fig. 6A, B), suggesting that activation of either receptor subtype can fully mediate the inhibitory effect. However, in a smaller subpopulation (<25%), the inhibition required concurrent activation of both M2 and M4 receptors, as only dual receptor blockade completely reversed the effect (Fig. 6C, D). These functional observations align with earlier studies showing that M2 and M4 receptors jointly regulate neurotransmitter release in striatal pathways[58,59]. The immunofluorescence evidence confirms the co-localization of both receptors on a proportion of 5-HT neurons, reinforcing the notion that M2 and M4 may act cooperatively in a subset of cells to modulate inhibitory responses.

Effects of muscarinic receptors on locomotion in brainstem

Cholinergic propriospinal neurons play an essential role in modulating CPG to generate locomotion[24,31,60–62]. Previous studies have shown that ACh induce coordinated fictive locomotion in the isolated whole spinal cord[29,63]. These studies demonstrated in neonatal rat preparations that facilitation of the endogenous cholinergic propriospinal system could initiate the coordinated locomotor activity, which could be blocked by mAChRs antagonist, especially M2 and M3 muscarinic receptors antagonist[30]. Recent studies further show that cholinergic intraspinal systems mediate balanced, multimodal control of spinal motor output through activation of M2 and M3 muscarinic receptors[31,34,35]. However, the role of acetylcholine, especially mAChRs in regulating locomotion in the midbrain is not clear, yet.

The pedunculopontine tegmental nucleus (PPT/Ch5) and laterodorsal tegmental nucleus (LDT/Ch6), as key cholinergic nuclei within the brainstem, project extensively to the MLR. Cholinergic modulation of locomotor control through this pathway involves three distinct mechanisms mediated by acetylcholine receptors (AChRs)[44]. AChRs expressed on MLR glutamatergic neurons regulate locomotor initiation and velocity through modulation of excitatory drive to CPG. Furthermore, mAChRs localized on dopaminergic neurons in the substantia nigra pars compacta (SNc) enhance both locomotor activity and reward-associated motor behaviors via facilitated dopamine release[56].

In contrast to direct synaptic regulation, mAChR-mediated locomotor control in the medulla operates through hierarchical circuitry. Studies in lampreys demonstrate that MLR cholinergic neurons modulate RSN not via direct mAChR innervation, but rather through intermediate "muscarinoceptive" neurons essential for rhythm generation[48]. This indirect regulatory architecture appears evolutionarily conserved, as evidenced by our findings in mammalian systems. We identified that ACh regulated 5-HT neuronal excitability in the ventral medulla via M2/M3/M4 receptor activation (Figs. 5–7), with cholinergic projections from PPN to medulla confirmed by retrograde tracing (Fig. 7B). Notably, these 5-HT neurons may constitute the mammalian homolog of lamprey muscarinoceptive interneurons, forming a parallel indirect pathway. Such interspecies parallels underscore the need for comparative studies to discern conserved principles from species-specific adaptations in cholinergic locomotor networks.

Previous studies in lampreys demonstrated that microinjection of the mAChRs antagonist atropine into brainstem regions significantly reduced swimming speed induced by electrical stimulation of the MLR[48], providing initial evidence for mAChRs-mediated regulation of step frequency in locomotor patterns. Subsequent investigations of respiratory control in rats revealed that M4 receptors within the pedunculopontine tegmental nucleus exerted inhibitory effects on respiratory rhythm generation[46]. These collective findings consistently implicated brainstem mAChRs in the modulation of rhythmic motor outputs. The present study extended these observations by systematically investigating the role of brainstem mAChRs in fictive locomotor rhythm generation. Utilizing both whole spinal cord ventral root recordings (Fig. 8) and computational modeling approaches (Fig. 9), we provided the first experimental evidence that pharmacological manipulation of brainstem mAChRs significantly modulated the frequency of fictive locomotor rhythm in mice (Fig. 10). This novel finding aligns with the earlier observations in lamprey swimming models, confirming the evolutionarily conserved nature of cholinergic modulation in brainstem-mediated locomotor control.

In rodent models, however, the PPN cholinergic neurons in locomotion initiation remains contentious[27]. Whereas some studies report no significant effect of PPN cholinergic neurons on locomotor initiation[64,65], others demonstrate their involvement in augmenting[36,66] or attenuating locomotor velocity[5]. Our findings reconciled these disparate observations by demonstrating that medullary muscarinic acetylcholine receptor (mAChR) subtypes differentially modulated locomotor output, as evidenced by in vitro isolated whole-spinal cord recordings (Fig. 8 and Supplementary Fig. 4). Consistent with triphasic responses to acetylcholine in medullary 5-HT neurons, Blockage of medullary M1/M5 receptors exerted no significant influence on locomotor rhythmogenesis (Supplementary Fig. 4). Conversely, blocking M3 receptor receptors reduced gait frequency and perturbated locomotion, whereas antagonizing M2/M4 receptors increased stepping frequency without altering locomotor pattern (Fig. 8). This study established a mechanistic framework whereby PPN cholinergic neurons facilitated locomotion through subtype-specific mAChR activation.

Limitations of the experiments

In this study, we found that 5-HT neurons in the medulla were concentrated on the PPR and MRN regions and that there was a significant morphological difference between these two regions (Fig. 1). More importantly, the cholinergic effects on 5-HT neurons in the PPR and MRN were quite different. Acetylcholine enhanced excitability of 5-HT neurons in the PPR, while ACh appeared to have little effect on the 5-HT neurons in the MRN. It was found in previous experiments that electrical stimulation of 5-HT neurons in the PPR region was more likely to induce fictive locomotion than stimulation of 5-HT neurons in the MRN[14]. Therefore, it is not clear whether the different

responses of 5-HT neurons to ACh in the PPR and MRN could determine their different roles in generating locomotion. A further study is required to address this issue in the future.

While our isolated spinal cord experiments establish the essential role of brainstem muscarinic receptors in locomotor control (Fig. 8), we acknowledge that muscarinic antagonists could also affect non-5-HT neuronal populations within the medulla. Nevertheless, multiple lines of evidence support a central role for the cholinergic–serotonergic pathway: (1) in vitro electrophysiology demonstrates direct acetylcholine-mediated modulation of 5-HT neuronal excitability via M2, M3, and M4 receptors (Figs. 5, 6); (2) immunohistochemical mapping confirms preferential co-expression of these receptors on 5-HT neurons in the ventral medulla (Fig. 7A); (3) retrograde tracing reveals MLR cholinergic terminals in close apposition to medullary 5-HT somata (Fig. 7B). Although substantial non-serotonergic neurons (GABAergic, glutamatergic, etc.) in this region also express muscarinic receptors[67], the converging evidence—combined with the established role of medullary 5-HT neurons in locomotor patterning[14], supports their function as key mediators of cholinergic modulation over spinal central pattern generators. Thus, the locomotor modulation observed likely reflects integrated multi-pathway actions, with serotonergic circuits serving as principal, but not exclusive contributors. Future studies using cell-type-specific manipulations during fictive locomotion will help dissect contributions from parallel circuits.

Furthermore, synaptic inputs to medullary 5-HT neurons were functionally represented by cholinergic components only in our model, with excitatory and inhibitory synaptic inputs representing M3 and M2/M4 receptor-mediated synaptic currents respectively. Although the present study employed a highly simplified neural network model, the modeling results not only validated our electrophysiological findings (Fig. 8) but also demonstrated that bidirectional manipulation of 5-HT neuronal activity (facilitation via M3-like inputs vs. suppression through M2/M4-type inhibition) significantly modulated fictive locomotor rhythm parameters. These computational predictions retained scientific validity as they mechanistically recapitulated the essential interplay between cholinergic and serotonergic systems within brainstem locomotor circuits under physiological conditions.

In this study the model was highly simplistic with focusing 5-HT as the only driver of the observed effects. Under physiological conditions, multiple neurotransmitters drive CPG networks to produce locomotion[29]. Our reduced-complexity model intentionally abstracted non-serotonergic mechanisms to isolate how brainstem cholinergic-serotonergic pathways reconfigure CPG output. Although this approach cannot fully replicate physiological complexity, it successfully demonstrated how muscarinic receptor modulation of 5-HT neuronal excitability regulates locomotor circuits. Extensive studies have shown previously that the neurotransmitter glutamate, particularly the NMDA receptors involved, plays a crucial role in the initiation and regulation of locomotion in the brainstem and spinal cord[16,27,68,69]. Therefore, future studies will incorporate NMDA receptor dynamics to elucidate the synergistic integration of glutamatergic, serotonergic and cholinergic modulations in vertebrate locomotor control.

Conclusions

Our findings reveal a synergistic antagonism within medullary cholinergic-serotonergic pathways, where M3 receptor-mediated excitation and M2/M4 receptor-dependent inhibition bidirectionally coordinate 5-HT neuronal excitability in *ePet-EYFP* mice. This receptor-specific reciprocity forms the core mechanistic basis for cholinergic-serotonergic interplay, through which brainstem circuits dynamically balance neuronal states and locomotor output. The functional synergy between opposing muscarinic signals (M3 vs. M2/M4) enables precise tuning of both rhythm generation and motor stability, establishing a dual-control system essential for adaptive locomotion.

Materials and methods

Animal model

Experiments were carried out in accordance with the East China Normal University Laboratory Animal Center and all procedures were in accordance with protocols approved by the Animal Experiment Ethics Committee (Ethics No. ARXM2025180). The experiments were carried out on neonatal *ePet-EYFP* mice (P3-P6), crossed by *ePet-Cre* mice (The Jackson Laboratory, stock no. 012712) with *R26-stop-EYFP* mice (The Jackson Laboratory, stock no. 006148), and neonatal *ChAT-IRES-EYFP* mice (P3-P6) crossed by *ChAT-IRES-Cre* mice (The Jackson Laboratory, stock no. 006410) with *R26-stop-EYFP* mice. *ePet-Cre* mice were used to drive Cre recombinase expression in 5-HT neurons via the Pet1 enhancer, enabling tissue-specific recombination when crossed with loxP-flanked strains. *R26-stop-EYFP* mice feature a loxP-flanked STOP cassette before EYFP at the ROSA26 locus, enabling Cre-dependent tissue-specific labeling *ChAT-IRES-Cre* knock-in mice enable Cre recombinase expression in cholinergic neurons without disrupting endogenous choline acetyltransferase (Chat) function.

Euthanasia methods were optimized per experimental paradigm: cervical dislocation with subsequent decapitation preserved medullary ultrastructure for patch-clamp/retrograde tracing studies, while direct ponto-medullary transection maintained brainstem-spinal cord continuity essential for ventral root recordings. Animals were exposed to a 12 h light/dark cycle and had free access to food and water. Their pain and distress were minimized.

Preparation of slices and patch-clamp recordings

The general experimental and surgical procedures have been described in details in previous studies[19]. The 3–6 days old *ePet-EYFP* mice of either sex were euthanized by cervical dislocation and quickly decapitated. To study 5-HT neurons, a section of medulla was removed and glued to a Plexiglas tray filled with cooled dissecting artificial cerebrospinal fluid (ACSF), bubbled with 95% O_2 + 5% CO_2. Four transverse slices of 200 μm thick were cut from the ponto-medullary junction, transferred to a holding chamber and incubated at room temperature (20–22 °C) for 30 min recover in recording ACSF.

Transferred slices to a recording chamber mounted in the stage of an upright Olympus BX50 microscope fitted with differential interference contrast (DIC) optics and epifluorescence. The chamber was perfused with recording ACSF at rate of 2 ml/min, bubbled with 95% O_2 + 5% CO_2. The $EYFP^+$ 5-HT neurons were identified at 40X magnification using epifluorescence with a narrow band YFP cube. The visualized $EYFP^+$ neurons were patched with glass pipette electrodes. The pipette electrodes were pulled from borosilicate glass (1B150F-4; WPI) with an electrode puller (P-1000; Sutter Instrument) and had resistances of 6–8 MΩ when filled with intracellular solution. tetramethylrhodamine (TMRM 3%) was added to the intracellular solution to study the morphology of the recorded 5-HT neurons. A MultiClamp 700B, a Digidata 1550, a MiniDigi 1B, and pCLAMP (10.7) (all from Molecular Devices) were used for data acquisition. Data were low-pass filtered at 3 kHz and sampled at 10 kHz. Whole cell patch recordings were made in voltage-clamp mode with capacitance compensation and current-clamp mode with bridge balance. All electrophysiological data were analyzed with Clampfit (10.7). The parameters measured and calculated in this study included the resting membrane potential (RMP), input resistance (Rin), current threshold (rheobase), action potential (AP) height and afterhyperpolarization (AHP) depth. Details of the calculation were described in previous studies[70].

Morphological analysis

For morphological analysis, a subset of EYFP-positive 5-HT neurons was patched and labeled using pipette electrodes filled with intracellular solution containing 3% TMRM. Following 5–10 min of staining, images of the labeled neurons were immediately acquired using a Nikon Eclipse Ni fluorescence microscope equipped with a Nikon DS-Ri2 color digital camera, at excitation wavelengths of 540–580 nm and 465–495 nm, respectively. Somatic parameters were quantified using Nikon NIS-Elements imaging software (v5.30), where somatic diameter (d) was calculated as the mean of minor and major axes. Somatic area and volume were calculated as πd^2 and $\pi d^3/6$, respectively. Dendritic

complexity was quantified using Sholl Analysis plugins (v3.6) in ImageJ (1.52 g) with concentric circles at 25 μm intervals centered on the soma centroid. Secondary morphological parameters (dendritic branches, terminals, and primary segments) were analyzed using the NeuronJ plugin (v1.4.3)[71].

Statistics and reproducibility

Statistical analysis was performed using GraphPad Prism 8.0. Data, obtained from multiple biological samples ($n \geq 6$), are presented as the mean ± SD of at least three independent experiments. The normality (Shapiro-Wilk test) and homoscedasticity (Levene's test) of data distributions were verified for all parametric tests. Comparisons between two groups were conducted with two-tailed unpaired t-tests, while one-way ANOVA was used for comparisons among three or more groups. Where the assumptions of parametric tests were violated, non-parametric alternatives (Kruskal-Wallis/Wilcoxon tests) were employed. A result was considered statistically significant at $^{*}P < 0.05$, $^{**}P < 0.01$, and $^{***}P < 0.001$.

Immunofluorescence

Immunostaining for M2, M3, and M4 receptors was performed on tissue sections fixed with 4% paraformaldehyde in phosphate buffer. For indirect immunofluorescence studies, cells were treated overnight with rabbit anti-M2 receptor antibody (ab41168, Abcam, Tokyo, Japan), rabbit anti-M3 receptor antibody (ab126168, Abcam, Tokyo, Japan), and rabbit anti-M4 receptor antibody (ab189432, Abcam, Tokyo, Japan). After incubation, the cells were washed three times with phosphate buffer saline and then treated with a respective secondary antibody conjugated with Alexa 488 or 546 (Molecular Probe, Eugene, OR, USA). The fluorescence was observed using a Nikon Eclipse Ni fluorescence microscopy (Nikon DS-Ri2 color, Japan). An oil-immersion objective lens with 60X magnification was used, and fluorescence was observed using appropriate laser lines and filter sets.

Solutions and chemicals

Dissecting ACSF (mM): NaCl (25), sucrose (253), KCl (1.9), NaH_2PO_4 (1.2), $MgSO_4$ (10), $NaHCO_3$ (26), kynurenic acid (1.5), glucose (25), and $CaCl_2$ (1.0).

Recording ACSF (mM): NaCl (125), KCl (2.5), $NaHCO_3$ (26), NaH_2PO_4 (1.25), glucose (25), $MgCl_2$ (1), and $CaCl_2$ (2.0).

Intracellular solution (mM): K-gluconate (135), NaCl (10), HEPES (10), $MgCl_2$ (2), Mg-ATP (5), and GTP (0.5).

The pH of these solutions was adjusted to 7.3 with HCl. Osmolarity was adjusted to 305 mOsm by adding sucrose to the solution.

Retrograde tracing

The specific procedure of the retrograde tracing experiment was basically consistent with that described in our previous studies[72,73]. ChAT-IRES-EYFP mice (P3-P6) of either sex were euthanized by cervical dislocation and quickly decapitated. A section of the brainstem was removed and glued to a Plexiglas tray. A 1.5 mm of vaseline wall was built at the pons, and then the area above the pons was filled with cooled recording ACSF, which was bubbled with 95% O_2 and 5% CO_2. The retrograde tracers (25% TMRM) were injected into the ventral area of medulla using a manual microinjection pump (WPI, MMP, USA), and the medulla was kept moist in recording ACSF. Slices of 200 μm of the midbrain were cut after 5 h labeling.

Whole spinal cord ventral root recording

Wild type mice (P3-P6) were euthanatized by decapitation, and their spinal cords were isolated by ventral laminectomy under ice-cold (4°C), oxygenated (95% O_2 + 5% CO_2) dissecting ACSF. The isolated medulla and spinal cord were removed and pinned ventral side-up and perfused with oxygenated recording ACSF. Vaseline was used to separate the spinal cord from the medulla in the cervical spine. Compartment integrity was verified by applying aCSF to the medullary side with 2-min observation. Only barrier systems showing no fluid transfer had aCSF added to the spinal cord region[72]. Experiments were performed after incubating preparations in oxygenated regular recording ACSF at room temperature (20–22 °C) for 30 min.

5-hydroxytryptamine (5-HT; 20–30 μM) and N-methyl-Daspartate (NMDA; 3-5 μM) were applied to the spinal cord area and muscarine (20 μM) were applied to medulla area to generate well-coordinated fictive locomotion, including alternation between the rL5 and lL5. The raw ENG recordings of the rL5 and lL5 ventral roots were recorded over a 40 s duration. The ENG data were then rectified and filtered for detailed analysis to determine the relationships between right/left activities. Polar plots, which were produced from the rectified and filtered waveforms, demonstrated the coordinated locomotor activities. When the drug significantly reduced or abolished the ENG amplitude, we selected events in the rectified and filtered waveform that were greater than 20% of the average fluctuation amplitude to calculate the frequency and coordinated of the fictive locomotion. Ventral root recordings were band-pass-filtered (100 to 5 kHz) and recorded using a MultiClamp 700B (Molecular Devices, Silicon Valley, CA, United States).

Modeling

A CPG network model was built with NEURON 7.7 (NEURON, Yale University, New Haven, CT, United States). General CPG network and neuronal simulations have been described in detail in previous studies[50]. Briefly, the CPG model consisted of left and right half-centers, each half-center consisted of 5 neurons and received synaptic inputs from two inhibitory commissural interneurons (CIN) pools. The output of the whole spinal network was initiated by a brief excitatory input delivered simultaneously to the left and right half-centers from the 5-HT neuron pool (see Supplementary Table 13 for details). The representative neurons from each half-center were selected to demonstrate rhythmic activity.

In order to reduce computing costs without losing simulation accuracy, we simplified the morphology of the neurons to a single compartment with conductances described by Hodgkin-Huxley equations. Each 5-HT neuron included the NaT (transient sodium), K(DR) (delayed rectifier potassium), K(AHP) (calcium-dependent potassium), CaL (L-type calcium) and potassium-mediated leak channels. The half-center neurons included CaL, NaT, K(DR), K(AHP), NaP (persistent sodium) and potassium-mediated leak channels. The membrane properties of the model neurons were based on previous research[74–76].

The membrane current equation for the 5-HT neurons and half-center models was given by

$$C_m \frac{dV_m}{dt} = -\sum I_{ion} - \sum I_{syn} + I_{stim} \tag{1}$$

where C_m, I_{ion}, I_{syn}, and I_{stm} were membrane capacitance, ion currents, synaptic currents, and stimulus currents, respectively. Ionic currents included

$$\begin{cases} I_{NaT} = g_{NaT} \cdot m^3 \cdot h \cdot (V_m - E_{Na}) \\ I_{K(DR)} = g_{K(DR)} \cdot n^4 \cdot (V_m - E_K) \\ I_{K(AHP)} = g_{K(AHP)} \cdot q \cdot (V_m - E_K) \\ I_{NaP} = g_{NaP} \cdot m \cdot s \cdot (V_m - E_{Na}) \\ I_{CaL} = g_{CaL} \cdot k \cdot (V_m - E_{Ca}) \\ I_{Leak} = g_{Leak}(V_m - E_{Leak}) \end{cases} \tag{2}$$

where g_{NaT}, $g_{K(DR)}$, $g_{K(AHP)}$, g_{NaP}, g_{CaL} and g_{Leak} were the maximum conductances for I_{NaT}, $I_{k(DR)}$, $I_{K(AHP)}$, I_{NaP}, I_{CaL}, and I_{Leak} respectively. E_{Na}, E_K, E_{Ca} and E_{Leak} were equilibrium potentials for Na^+, K^+, Ca^{2+}, and Leak currents and were set to 55 mV, −75mV, 80 mV and −75mV, respectively. The resting membrane potential (RMP) of the model cells was set to −65 mV. m, h, n, s and k were state variables that were defined by a Hodgkin-

Huxley equation:

$$\frac{dX}{dt} = \alpha(1 - X) - \beta X \quad (3)$$

where α and β were rate constants for NaT, NaP, and K(DR) ion channels (Supplementary Table 14) and were adjusted to reflect the kinetics of spinal neurons[74]. The conductances for NaT, NaP, K(DR), and leak channels were chosen based on a combination of previous CPG model[77] and motoneuron model[74,78,79].

The intracellular calcium concentration ($[Ca^{2+}]_{in}$) in the compartment satisfied the following equation:

$$\frac{d[Ca^{2+}]_{in}}{dt} = B \cdot I_{CaL} - \frac{[Ca^{2+}]_{in}}{\tau_{Ca}} \quad (4)$$

where B was a scaling constant set to 10. τ_{Ca} was a time constant, the rate of decay of $[Ca^{2+}]_{in}$ and was set to 15 ms. I_{CaL} was the L-type Ca^{2+} current.

The following mathematical model represented the inhibitory and excitatory synaptic currents between half-center neurons (reciprocal inhibitory synapse)

$$\begin{cases} I_{\mathrm{Exc}}(t) = g_{\mathrm{Exc}} \cdot (e^{-(t-t_0)/\tau_1} - e^{-(t-t_0)/\tau_2}) \cdot (V_m - E_{\mathrm{Exc}}) \\ I_{\mathrm{Inh}}(t) = g_{\mathrm{Inh}} \cdot (e^{-(t-t_0)/\tau_1} - e^{-(t-t_0)/\tau_2}) \cdot (V_m - E_{\mathrm{Inh}}) \end{cases} \quad (5)$$

where the maximum conductance g_{Exc} and g_{Inh} were set to about 0.1 μS/ cm^2. The equilibrium potential of E_{Exc} and E_{Inh} was set to 0 and -80 mV, respectively. The time constants of τ_1 and τ_2 were set to 0.01 ms, and 0.05 ms, respectively. To simulate the temporal and spatial integration properties of synapses, we incorporated additional excitatory and inhibitory synaptic inputs to each neuron, with synaptic weights and time constants following a uniform distribution.

Reporting summary

Further information on research design is available in the Nature Portfolio Reporting Summary linked to this article.

Data availability

All source data underlying the graphs and charts presented in the main figures is uploaded in Supplementary Table and Supplementary Data 1.

Code availability

The neural network model code is available from the corresponding authors upon reasonable request.

Received: 4 June 2025; Accepted: 10 November 2025;
Published online: 25 November 2025

References

1. Grillner, S. & El Manira, A. Current principles of motor control, with special reference to vertebrate locomotion. *Physiol. Rev.* **100**, 271–320 (2020).
2. Kiehn, O. Decoding the organization of spinal circuits that control locomotion. *Nat. Rev. Neurosci.* **17**, 224–238 (2016).
3. Goulding, M. Circuits controlling vertebrate locomotion: moving in a new direction. *Nat. Rev. Neurosci.* **10**, 507–518 (2009).
4. Goñi-Erro, H., Selvan, R., Leiras, R. & Kiehn, O. Pedunculopontine Chx10(+) neurons control global motor arrest in mice. *Nat. Neurosci*. https://doi.org/10.1038/s41593-023-01396-3 (2023).
5. Caggiano, V. et al. Midbrain circuits that set locomotor speed and gait selection. *Nature* **553**, 455–460 (2018).
6. Musienko, P. E. et al. Spinal and supraspinal control of the direction of stepping during locomotion. *J. Neurosci.* **32**, 17442-17453(2012).
7. Opris, I. et al. Activation of brainstem neurons during mesencephalic locomotor region-evoked locomotion in the cat. *Front. Syst. Neurosci.* **13**, 69 (2019).
8. Harris-Warrick, R. M. General principles of rhythmogenesis in central pattern generator networks. *Prog. Brain Res.* **187**, 213–222 (2010).
9. Kiehn, O. Development and functional organization of spinal locomotor circuits. *Curr. Opin. Neurobiol.* **21**, 100–109 (2011).
10. Dai, X., Noga, B. R., Douglas, J. R. & Jordan, L. M. Localization of spinal neurons activated during locomotion using the c-fos immunohistochemical method. *J. Neurophysiol.* **93**, 3442–3452 (2005).
11. Jordan, L. M., Liu, J., Hedlund, P. B., Akay, T. & Pearson, K. G. Descending command systems for the initiation of locomotion in mammals. *Brain Res. Rev.* **57**, 183–191 (2008).
12. Chopek, J. W., Zhang, Y. & Brownstone, R. M. Intrinsic brainstem circuits comprised of Chx10-expressing neurons contribute to reticulospinal output in mice. *J. Neurophysiol.* **126**, 1978–1990 (2021).
13. Bretzner, F. & Brownstone, R. M. Lhx3-Chx10 reticulospinal neurons in locomotor circuits. *J. Neurosci.* **33**, 14681–14692 (2013).
14. Liu, J. & Jordan, L. M. Stimulation of the parapyramidal region of the neonatal rat brain stem produces locomotor-like activity involving spinal 5-HT7 and 5-HT2A receptors. *J. Neurophysiol.* **94**, 1392–1404 (2005).
15. Sławińska, U. & Jordan, L. M. Serotonergic influences on locomotor circuits. *Curr. Opin. Physiol.* **8**, 63–69 (2019).
16. Cazalets, J. R., Sqalli-Houssaini, Y. & Clarac, F. Activation of the central pattern generators for locomotion by serotonin and excitatory amino acids in neonatal rat. *J. Physiol.* **455**, 187–204 (1992).
17. Sławińska, U. et al. Unusual quadrupedal locomotion in rat during recovery from lumbar spinal blockade of 5-HT(7) receptors. *Int. J. Mol. Sci.* **600722**, 6007 (2021).
18. Noga, B. R., Johnson, D. M., Riesgo, M. I. & Pinzon, A. Locomotor-activated neurons of the cat. I. Serotonergic innervation and co-localization of 5-HT7, 5-HT2A, and 5-HT1A receptors in the thoraco-lumbar spinal cord. *J. Neurophysiol.* **102**, 1560–1576 (2009).
19. Cheng, Y., Song, N., Ge, R. & Dai, Y. Serotonergic modulation of persistent inward currents in serotonergic neurons of medulla in ePet-EYFP mice. *Front. Neural Circuits* **15**, 657445 (2021).
20. Chen, K., Ge, X. & Dai, Y. Cholinergic modulation of persistent inward currents is mediated by activating muscarinic receptors of serotonergic neurons in the brainstem of ePet-EYFP mice. *Exp. Brain Res.* **240**, 1177–1189 (2022).
21. Cheng, Y., Zhang, Q. & Dai, Y. Sequential activation of multiple persistent inward currents induces staircase currents in serotonergic neurons of medulla in ePet-EYFP mice. *J. Neurophysiol.* **123**, 277–288 (2020).
22. Cheng, Y. et al. Multiple patterns of persistent inward currents with multiple types of repetitive firings in medullary serotonergic neurons of mice: an experimental and modeling study. *PLoS Comput. Biol.* **21**, e1012918 (2025).
23. Harris-Warrick, R. M. Neuromodulation and flexibility in Central Pattern Generator networks. *Curr. Opin. Neurobiol.* **21**, 685–692 (2011).
24. Kiehn, O. et al. Excitatory components of the mammalian locomotor CPG. *Brain Res. Rev.* **57**, 56–63 (2008).
25. Milla-Cruz, J. J. et al. The activation of D(2) and D(3) receptor subtypes inhibits pathways mediating primary afferent depolarization (PAD) in the mouse spinal cord. *Neurosci. Lett.* **736**, 135257 (2020).
26. Bryson, M. et al. Emergent epileptiform activity in spinal sensory circuits drives ectopic bursting in afferent axons and sensory dysfunction after cord injury. *Pain* **166**, e27–e35 (2025).
27. Leiras, R., Cregg, J. M. & Kiehn, O. Brainstem circuits for locomotion. *Annu Rev. Neurosci.* **45**, 63–85 (2022).

28. Shreckengost, J. et al. Nicotinic receptor modulation of primary afferent excitability with selective regulation of Aδ-mediated spinal actions. *J. Neurophysiol.* **125**, 568–585 (2021).
29. Cowley, K. C. & Schmidt, B. J. A comparison of motor patterns induced by N-methyl-D-aspartate, acetylcholine and serotonin in the in vitro neonatal rat spinal cord. *Neurosci. Lett.* **171**, 147–150 (1994).
30. Jordan, L. M. et al. Cholinergic mechanisms in spinal locomotion-potential target for rehabilitation approaches. *Front. Neural Circuits* **8**, 132 (2014).
31. Miles, G. B., Hartley, R., Todd, A. J. & Brownstone, R. M. Spinal cholinergic interneurons regulate the excitability of motoneurons during locomotion. *Proc. Natl. Acad. Sci. USA* **104**, 2448–2453 (2007).
32. Kissane, R. W. P. et al. C-bouton components on rat extensor digitorum longus motoneurons are resistant to chronic functional overload. *J. Anat.* **241**, 1157–1168 (2022).
33. Mille, T., Quilgars, C., Cazalets, J. R. & Bertrand, S. S. Acetylcholine and spinal locomotor networks: the insider. *Physiol. Rep.* **9**, e14736 (2021).
34. Nascimento, F. et al. Synaptic mechanisms underlying modulation of locomotor-related motoneuron output by premotor cholinergic interneurons. *Elife* **9**, https://doi.org/10.7554/eLife.54170 (2020).
35. Nascimento, F., Spindler, L. R. B. & Miles, G. B. Balanced cholinergic modulation of spinal locomotor circuits via M2 and M3 muscarinic receptors. *Sci. Rep.* **9**, 14051 (2019).
36. Xiao, C. et al. Cholinergic mesopontine signals govern locomotion and reward through dissociable midbrain pathways. *Neuron* **90**, 333–347 (2016).
37. Sholomenko, G. N., Funk, G. D. & Steeves, J. D. Avian locomotion activated by brainstem infusion of neurotransmitter agonists and antagonists. *I. Acetylcholine Excitatory Amino Acids Subst. P. Exp. Brain Res.* **85**, 659–673 (1991).
38. Bertrand, S. S. & Cazalets, J. R. Cholinergic partition cells and lamina x neurons induce a muscarinic-dependent short-term potentiation of commissural glutamatergic inputs in lumbar motoneurons. *Front. Neural Circuits* **5**, 15 (2011).
39. Sourioux, M., Bertrand, S. S. & Cazalets, J. R. Cholinergic-mediated coordination of rhythmic sympathetic and motor activities in the newborn rat spinal cord. *PLoS Biol.* **16**, e2005460 (2018).
40. Dautan, D. et al. Cholinergic midbrain afferents modulate striatal circuits and shape encoding of action strategies. *Nat. Commun.* **11**, 1739 (2020).
41. Akyuz, E. et al. Immunoreactivity of Kir3.1, muscarinic receptors 2 and 3 on the brainstem, vagus nerve and heart tissue under experimental demyelination. *Brain Res. Bull.* **197**, 13–30 (2023).
42. Yeomans, J. S. Muscarinic receptors in brain stem and mesopontine cholinergic arousal functions. *Handb. Exp. Pharmacol*. 243-259, (2012).
43. Dai, Y. & Jordan, L. M. in *Society for Neuroscience (SFN)* (2014).
44. Ishii, M. & Kurachi, Y. Muscarinic acetylcholine receptors. *Curr. Pharm. Des.* **12**, 3573–3581 (2006).
45. Zhang, H. M. et al. Opposing functions of spinal M2, M3, and M4 receptor subtypes in regulation of GABAergic inputs to dorsal horn neurons revealed by muscarinic receptor knockout mice. *Mol. Pharm.* **69**, 1048–1055 (2006).
46. Lima, J. D., Sobrinho, C. R., Santos, L. K., Takakura, A. C. & Moreira, T. S. M4-muscarinic acetylcholine receptor into the pedunculopontine tegmental nucleus mediates respiratory modulation of conscious rats. *Respir. Physiol. Neurobiol.* **269**, 103254 (2019).
47. Roussel, M., Lafrance-Zoubga, D., Josset, N., Lemieux, M. & Bretzner, F. Functional contribution of mesencephalic locomotor region nuclei to locomotor recovery after spinal cord injury. *Cell Rep. Med.* **4**, 100946 (2023).
48. Smetana, R., Juvin, L., Dubuc, R. & Alford, S. A parallel cholinergic brainstem pathway for enhancing locomotor drive. *Nat. Neurosci.* **13**, 731–738 (2010).
49. Le Ray, D., Bertrand, S. S. & Dubuc, R. Cholinergic modulation of locomotor circuits in vertebrates. *Int. J. Mol. Sci.* **23** (2022).
50. Zhang, Q., Cheng, Y., Zhou, M. & Dai, Y. Locomotor pattern and force generation modulated by ionic channels: a computational study of spinal networks underlying locomotion. *Front. Comput. Neurosci.* **16**, 809599 (2022).
51. Picciotto, M. R., Higley, M. J. & Mineur, Y. S. Acetylcholine as a neuromodulator: cholinergic signaling shapes nervous system function and behavior. *Neuron* **76**, 116–129 (2012).
52. Wess, J. Novel insights into muscarinic acetylcholine receptor function using gene targeting technology. *Trends Pharm. Sci.* **24**, 414–420 (2003).
53. Tsimpili, H. & Zoidis, G. A new era of muscarinic acetylcholine receptor modulators in neurological diseases, cancer and drug abuse. *Pharmaceuticals* **18**, https://doi.org/10.3390/ph18030369 (2025).
54. Kaoullas, M. G., Thal, D. M., Christopoulos, A. & Valant, C. Ligand bias at the muscarinic acetylcholine receptor family: opportunities and challenges. *Neuropharmacology* **258**, 110092 (2024).
55. Levey, A. I. Immunological localization of m1-m5 muscarinic acetylcholine receptors in peripheral tissues and brain. *Life Sci.* **52**, 441–448 (1993).
56. Moehle, M. S. et al. Cholinergic projections to the substantia Nigra Pars reticulata inhibit dopamine modulation of basal ganglia through the M(4) muscarinic receptor. *Neuron* **96**, 1358–1372.e1354 (2017).
57. Yasuda, R. P. et al. Development of antisera selective for m4 and m5 muscarinic cholinergic receptors: distribution of m4 and m5 receptors in rat brain. *Mol. Pharm.* **43**, 149–157 (1993).
58. Ztaou, S. & Amalric, M. Contribution of cholinergic interneurons to striatal pathophysiology in Parkinson's disease. *Neurochem. Int.* **126**, 1–10 (2019).
59. Nunes, E. J., Addy, N. A., Conn, P. J. & Foster, D. J. Targeting the actions of muscarinic receptors on dopamine systems: new strategies for treating neuropsychiatric disorders. *Annu. Rev. Pharm. Toxicol.* **64**, 277–289 (2024).
60. Kiehn, O. Locomotor circuits in the mammalian spinal cord. *Annu. Rev. Neurosci.* **29**, 279–306 (2006).
61. Wilson, J. M., Rempel, J. & Brownstone, R. M. Postnatal development of cholinergic synapses on mouse spinal motoneurons. *J. Comp. Neurol.* **474**, 13–23 (2004).
62. Rozani, I. et al. Pitx2 cholinergic interneurons are the source of C bouton synapses on brainstem motor neurons. *Sci. Rep.* **9**, 4936 (2019).
63. Nistri, A. Effect of atropine and oxotremorine on the release of acetylcholine from the frog spinal cord. *Naunyn Schmiedebergs Arch. Pharm.* **295**, 89–94 (1976).
64. Josset, N. et al. Distinct contributions of mesencephalic locomotor region nuclei to locomotor control in the freely behaving mouse. *Curr. Biol.* **28**, 884–901.e883 (2018).
65. Kroeger, D. et al. Cholinergic, glutamatergic, and GABAergic neurons of the pedunculopontine tegmental nucleus have distinct effects on sleep/wake behavior in mice. *J. Neurosci.* **37**, 1352–1366 (2017).
66. Roseberry, T. K. et al. Cell-type-specific control of brainstem locomotor circuits by basal ganglia. *Cell* **164**, 526–537 (2016).
67. Lin, M. et al. A cholinergic spinal pathway for the adaptive control of breathing. *bioRxiv*, https://doi.org/10.1101/2025.01.20.633641 (2025).
68. Sqalli-Houssaini, Y., Cazalets, J. R. & Clarac, F. Oscillatory properties of the central pattern generator for locomotion in neonatal rats. *J. Neurophysiol.* **70**, 803–813 (1993).
69. MacLean, J. N., Cowley, K. C. & Schmidt, B. J. NMDA receptor-mediated oscillatory activity in the neonatal rat spinal cord is serotonin dependent. *J. Neurophysiol.* **79**, 2804–2808 (1998).
70. Dai, Y. et al. Electrophysiological and pharmacological properties of locomotor activity-related neurons in cfos-EGFP mice. *J. Neurophysiol.* **102**, 3365–3383 (2009).

71. Meijering, E. et al. Design and validation of a tool for neurite tracing and analysis in fluorescence microscopy images. *Cytom. A* **58**, 167–176 (2004).
72. Cheng, Y., Ge, R., Chen, K. & Dai, Y. Modulation of NMDA-mediated intrinsic membrane properties of ascending commissural interneurons in neonatal rat spinal cord. *J. Integr. Neurosci.* **18**, 163–172 (2019).
73. Carlin, K. P., Dai, Y. & Jordan, L. M. Cholinergic and serotonergic excitation of ascending commissural neurons in the thoraco-lumbar spinal cord of the neonatal mouse. *J. Neurophysiol.* **95**, 1278–1284 (2006).
74. Dai, Y., Jones, K. E., Fedirchuk, B., McCrea, D. A. & Jordan, L. M. A modelling study of locomotion-induced hyperpolarization of voltage threshold in cat lumbar motoneurones. *J. Physiol.* **544**, 521–536 (2002).
75. Rybak, I. A., Shevtsova, N. A., St-John, W. M., Paton, J. F. & Pierrefiche, O. Endogenous rhythm generation in the pre-Bötzinger complex and ionic currents: modelling and in vitro studies. *Eur. J. Neurosci.* **18**, 239–257 (2003).
76. Dixon, R. E., Navedo, M. F., Binder, M. D. & Santana, L. F. Mechanisms and physiological implications of cooperative gating of clustered ion channels. *Physiol. Rev.* **102**, 1159–1210 (2022).
77. Rybak, I. A., Shevtsova, N. A., Lafreniere-Roula, M. & McCrea, D. A. Modelling spinal circuitry involved in locomotor pattern generation: insights from deletions during fictive locomotion. *J. Physiol.* **577**, 617–639 (2006).
78. Dai, Y., Cheng, Y., Fedirchuk, B., Jordan, L. M. & Chu, J. Motoneuron output regulated by ionic channels: a modeling study of motoneuron frequency-current relationships during fictive locomotion. *J. Neurophysiol.* **120**, 1840–1858 (2018).
79. Binder, M. D., Powers, R. K. & Heckman, C. J. Nonlinear input-output functions of motoneurons. *Physiology* **35**, 31–39 (2020).

Acknowledgements

The authors sincerely thank Dr. Larry Jordan for proposing early plan for this study. This study is supported by National Nature Science Foundation of China (Grant No. 32471187, No. 32171129) to Y.D. and China Postdoctoral Science Foundation to Y.C. (2023M731112) and NSFC to R.G. (32260216).

Author contributions

Y.D. proposed the research; Y.C., Y.D. and R.G. performed experiments; Q.Z. did modeling; Y.D. and Y.C. drafted the manuscript; Y.D. and Y.C. edited and finalized the manuscript; All authors contributed to editorial changes in the manuscript and approved the submitted version.

Competing interests

The authors declare no competing interests.

Additional information

Supplementary information The online version contains supplementary material available at https://doi.org/10.1038/s42003-025-09217-y.

Correspondence and requests for materials should be addressed to Yue Dai.

Peer review information *Communications Biology* thanks the anonymous reviewers for their contribution to the peer review of this work. Primary Handling Editors: Claudia Kathe and Jasmine Pan. A peer review file is available.